Materials Today Energy 59 (2026) 102300

Contents lists available at ScienceDirect

Materials Today Energy

journal homepage: www.journals.elsevier.com/materials-today-energy/

SnO_x contact engineering in perovskite solar cells: Oxygen-Defect and valence control from selective to ambipolar transport

Neeraja Bose [a,1], Kumar GokulKumar [a,1], Shih Hsuan Chen [a,1], Kun Mu Lee [a,b,c,d,*]

[a] Department of Chemical and Materials Engineering, Chang Gung University, Taoyuan, 33302, Taiwan
[b] Center for Sustainability and Energy Technologies, Chang Gung University, Taoyuan, 33302, Taiwan
[c] Division of Neonatology, Department of Pediatrics, Chang Gung Memorial Hospital, Linkou, Taoyuan, 33305, Taiwan
[d] College of Environmental Science, Ming Chi University of Technology, New Taipei City, 24301, Taiwan

ARTICLE INFO

Keywords:
Tin oxide
Mixed valence (Sn^{2+}/Sn^{4+})
Electron transport layer (ETL)
Hole transport layer (HTL)
Ambipolar transport
Oxygen vacancy
Recombination
And interfacial stability

ABSTRACT

Tin oxide-based transport layers are crucial to high-performance perovskite solar cells (PSCs) because they potentially control non-radiative recombination, hysteresis, and long-term operation drift. SnO_x non-stoichiometry is significant because of its mixed-valence chemistry (Sn^{2+}/Sn^{4+}) and oxygen-related defect points, which can tune it to shift from electron-selective to hole-selective behavior. SnO_x can function as an ambipolar transport layer for interconnection/recombination upon careful control. However, the field lacks a clear, consistent understanding of (i) valence state distribution, (ii) defect density and surface chemistry, and (iii) processing control knobs for electronic properties and device outcomes. This review bridges the gap by evaluating the structure, electronic properties, and deposition routes of SnO, SnO_2, and intermediate valence SnO_x, and by mapping how SnO_x functions as ETL, HTL, and ambipolar/interlayer contact. We also discuss stability, degradation mechanism, and reliability issues linked to ambipolar SnO_x contacts and give guidance to validate and deploy SnO_x as a universal contact platform in PSCs. Overall, we define a design rule: oxygen activity controls the Sn^{2+}/Sn^{4+} balance and oxygen defect landscape, which determines the function of SnO_x as ETL, HTL, or an ambipolar interlayer with a narrow measurable defect window.

1. Introduction

Through the decades, perovskite solar cells (PSCs) have been known as a promising photovoltaic technology, with power conversion efficiencies crossing 26% in single-junction devices and 33% in tandem architectures. This progress is attributed to the optoelectronic properties of metal halide perovskites, including high absorption coefficients, long carrier diffusion lengths, and defect tolerance. Research focus has shifted from maximizing power conversion efficiency to addressing interfacial losses, defect passivation, and long-term operation stability in PSCs [1–3]. The major challenge for PSCs is the fabrication and optimization of the charge transport layers (CTLs) and their interface with perovskite absorbers. In conventional n-i-p and p-i-n architectures, the electron transport layers (ETLs) and hole transport layers (HTLs) control the charge extraction, recombination losses, hysteresis behavior, and long-term operational reliability. Several studies reported that device degradation and efficiency losses are continuously initiated by the buried CTL/perovskite interfaces rather than the perovskite bulk itself [4–6].

Eventually, the need for developing a chemically robust, energetically well-aligned, and defect-tolerant transport layer has become increasingly urgent. Metal oxide transport layers have gained attention due to their thermal stability, optical transparency, and compatibility with low-temperature processing. The tin oxide (SnO_2) can replace TiO_2 in planar PSCs as ETL because of its higher electron mobility, reduced photocatalytic activity, and improved band alignment with iodide-based perovskite [7–9]. Tin oxides are a broader material family that includes SnO (Sn^{2+}), SnO_2 (Sn^{4+}), and a range of non-stoichiometric intermediates (SnO_x, $1<x<2$). These phases stand out for their crystal structure, defect chemistry, and electronic properties. It is reported that non-stoichiometric SnO_x shows a high tunable electronic behavior, observed with mixed Sn^{2+}/Sn^{4+} valence states and oxygen vacancy populations. By adjusting its composition, defects, and interfaces, SnOx functions as an electron-, hole-, and ambipolar-transport layer. Due to its

* Corresponding authorDepartment of Chemical and Materials Engineering, Chang Gung University, Taoyuan-33302, Taiwan
E-mail address: kmlee@mail.cgu.edu.tw (K.M. Lee).
[1] All the authors have equally contributed.

https://doi.org/10.1016/j.mtener.2026.102300
Received 16 February 2026; Received in revised form 22 March 2026; Accepted 27 April 2026
Available online 27 April 2026

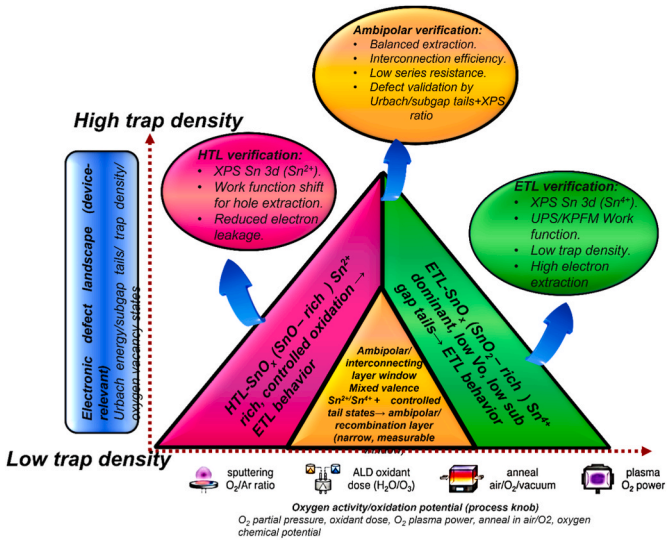

Fig. 1. Design rule for SnO_x contact functionality.

ability to enable ambipolarity, SnO_x can efficiently act as an HTL in p-i-n architecture and as a multifunctional recombination or interconnecting layer in tandem solar cells [10–12]. Such versatility is uncommon among inorganic transport materials, and underpins the use of SnO_x as a tunable and effective contact platform for PSCs architecture.

Ambipolar SnO_x is a non-stoichiometric tin oxide with mixed-valence Sn^{2+}/Sn^{4+} chemistry and oxygen defect states that produce electronic characteristics that enable transport of both electrons and holes under operating conditions. In PSCs, this supports interconnecting/recombination layers, which collect electrons from one sub-cell and holes from the other with low series resistance and reduced interfacial loss [13]. Ambipolarity is not a universal property; it occurs only in controlled process/composition windows where subgap tail states and defects are regulated and are essential for stable performance. Despite its benefits, the ambipolar SnO_x also has challenges, which can introduce defect-mediated recombination, energetic disorder, and time-dependent drift due to its mixed valence and oxygen-deficient chemistry. Also, the stability against oxidation, sensitivity towards transport polarity, and reproducibility of Sn^{2+}/Sn^{4+} of Sn^{2+} rich SnO-like HTL on deposition techniques are still under research. However, there are several literatures reported based on efficiency performance by SnO_2-rich SnO_x ETLs, whereas the activity of SnO_x as HTL and ambipolar interlayer is unexplored and lacks fabrication rules that link composition to device-relevant metrics such as band alignment, contact resistivity, and long-term stability.

Addressing these gaps is essential for translating lab scale demonstration into reliable device technologies. This review presents a focused discussion on ambipolar SnOx thin films of PSCs, covering i) crystals and electronic fundamentals, ii) depositions and fabrication strategies, and iii) functional roles as ETLs, HTLs, and interconnecting (recombination) layers. We bridge processing-controlled chemistry, specifically oxygen activity driving oxygen vacancy formation and Sn^{2+}/Sn^{4+} regulation to band alignment, charge selectivity, and dominant degradation pathways in n-i-p and p-i-n structures. Altogether, SnO_x can be engineered as a single, versatile contact platform for next-generation PSCs. Design rule for SnO_x contact functionality is illustrated in Fig. 1.

2. Fundamentals of SnO_2, SnO and SnO_x

2.1. Crystal structure and composition of SnO, SnO_2, and SnO_x layers

SnO belongs to a broader family of tin oxides, including SnO (Sn^{2+}), SnO_2 (Sn^{4+}), and non-stoichiometric intermediates SnO_x, which contain mixed-valence tin and varying degrees of oxygen-vacancy disorder. Stoichiometric SnO crystallizes in a layered tetragonal litharge structure, where each Sn atom is coordinated by four O atoms in a square pyramidal geometry [13]. This anisotropic arrangement produces quasi-2D electronic states with pronounced in-plane dispersion and out-of-plane localization, thereby facilitating intrinsic p-type transport arising from the Sn 5s/5p–O 2p antibonding hybridization [14]. In contrast, SnO_2 adopts the rutile structure, where six O^{2-} anions octahedrally coordinate each Sn^{4+} cation. Bulk SnO_2 is a transparent n-type semiconductor with a wide band gap, typically reported as 3.6–4.0 eV [15], although fundamental or electronic gap interpretation often

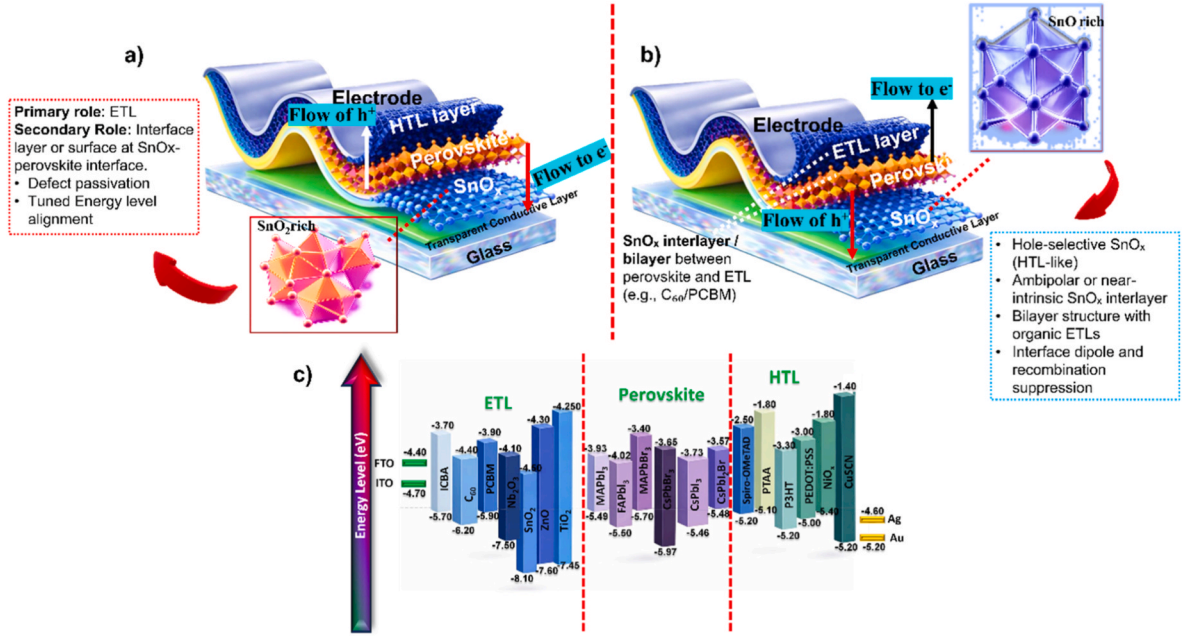

Fig. 2. Schematic illustration on scope of SnO_x in PSC device architectures: a) SnO_2-rich SnO_x as ETL, role and the charge flow; b) SnO-rich SnO_x as HTL, role and the charge flow; and c) The band alignment representation across ETL, HTL, and perovskite layers.

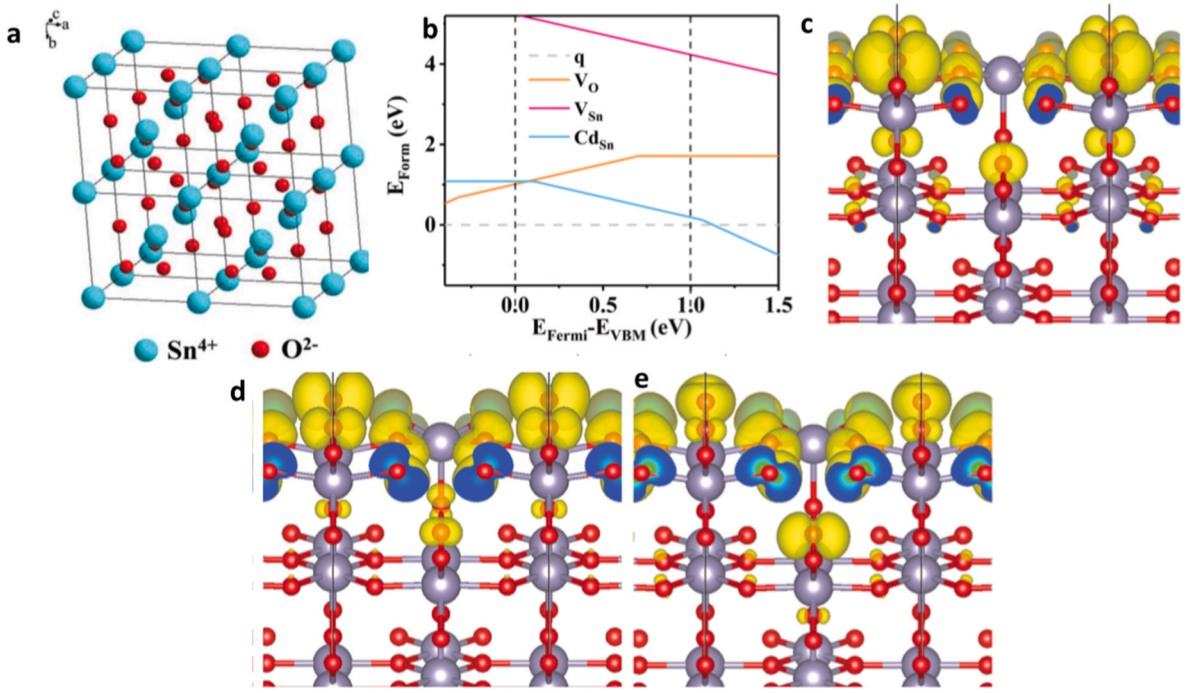

Fig. 3. Fundamentals of SnO_2 a) Crystalline arrangement, b) defect type and defect formation energy of pristine SnO_2, and c-e) Three mid gap orbitals of V_{sn} defect models [23].

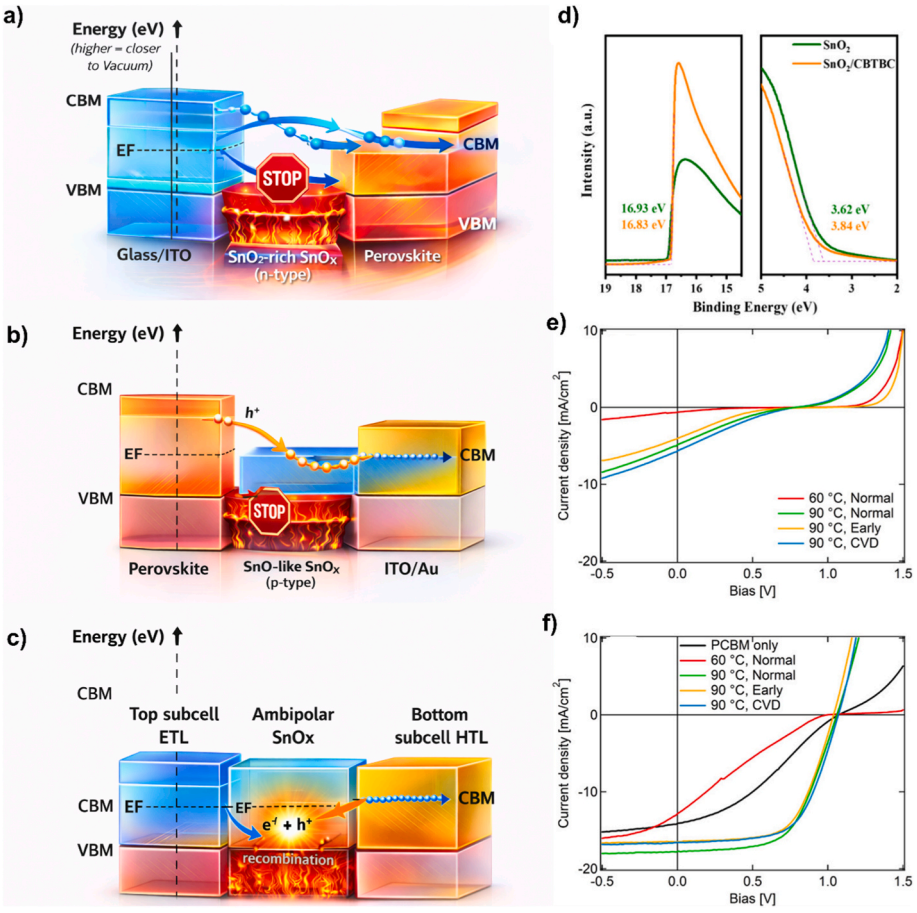

Fig. 4. a-c) Conceptual illustration of energy level diagram on SnO_2-rich SnO_x, SnO-rich SnO_x, and SnO_x as interlayer or recombination layer, d-f) UPS spectral on SnO_2 and *J-V* measurement curve of SnO_x as p-i-n PSC are reused from Refs. [28,29], Copyright © 2024, American Chemical Society.

Table 1
Oversight into the primary properties of SnO, SnO_2, and SnO_x.

Phase	Crystal Structure	Oxidation State	Bandgap (Eg)	Orbital Character	Intrinsic Transport Tendency	Significance of Ambipolar SnO_x	Current Challenges
SnO	Tetragonal litharge (*P4/nmm*); layered	Sn^{2+}	Indirect ≈ 0.6–0.8 eV; optical ≈ 2.6–2.8 eV	VBM: strong Sn 5s–O 2p antibonding (lone-pair driven); CBM: Sn 5p/O 2p	p-type (Sn vacancies as shallow acceptors, dispersive VB → low hole effective mass)	Provides p-type / hole-transport character; Sn 5s–O 2p hybridization is the origin of ambipolarity.	Stabilization of pure SnO, prevent conversion to SnO_2 or mixed phases, and obtaining reproducible p-type contacts with increased mobility at low temperatures.
SnO_2	Rutile (*P4₂/mnm*); 3D octahedral network	Sn^{4+}	Fundamental ≈ 3.0 eV; optical ≈ 3.6–4.0 eV	CBM: Sn 5s–O 2p antibonding; VBM: mainly O 2p	n-type (O vacancies and donor dopants → shallow donors, high electron mobility)	Acts as a classic ETL: deep VB blocks holes; CB alignment with perovskite and efficient electron extraction.	Reduction of defect-related traps (oxygen vacancy / Sn^{2+}, improving SnO_2 or active layer interface, procuring high performance with low temperature film with good reproducibility and scalability
SnO_x ($1<x<2$)	Mixed / nanocrystalline SnO + SnO_2; often partially amorphous	Mixed Sn^{2+}/ Sn^{4+} (plus O vacancies)	E_g tunable between SnO and SnO_2 limits; often 1–3 eV with mid-gap states	Mixed contributions: Sn 5s–O 2p at VBM and CBM; additional defect-related states (V_O, Sn^{2+}/ Sn^{4+} interfaces)	n-type, p-type or ambipolar, depending on Sn^{2+}/Sn^{4+} ratio and defect chemistry	Simultaneous electron and hole transport by tuning stoichiometry and vacancies.	Control of non-stoichiometry or Sn^{2+}/Sn^{4+} ratio by balancing conductivity, band alignment, and defect density for reproducible device performance

converges near ~3.0 eV and is method dependent. The n-type behavior originates primarily from intrinsic and extrinsic oxygen vacancies, as well as donor-like defects.

Non-stoichiometric SnO_x thin films produced by sputtering, ALD, or thermal oxidation generally contain nanocrystalline or amorphous mixtures of SnO-rich and SnO_2-rich regions. Their exact phase composition and crystallinity are susceptible to oxygen partial pressure, sputtering power, growth temperature, and post-annealing conditions, all of which dictate the average Sn^{2+}/Sn^{4+} ratio and oxygen-vacancy concentration [16]. At low deposition temperatures (40–120 °C), SnO_x films typically undergo a progressive oxidation, transitioning from mixed-valence Sn^{2+}/Sn^{4+} states toward a more Sn^{4+}-rich composition as the temperature increases. This process is accompanied by film densification, suppression of oxygen vacancies, and improved structural order [17]. Through such defect and valence engineering, SnO_x layers can be tailored to exhibit n-type ETL behavior, p-type HTL behavior, or fully ambipolar transport, enabling versatile integration in perovskite solar cells as illustrated in Fig. 2.

2.2. Chemistry and defect physics

2.2.1. SnO mixed-valence chemistry and lone-pair effects

SnO has an electronic structure dominated by a stereochemically active Sn $5s^2$ lone pair, which is strongly hybridized with O 2p states at the top of the valence band to form antibonding states as in Fig. S1 [18]. First-principles calculations and spectroscopic data indicate that SnO possesses a small indirect band gap of ~0.7 eV and a larger optical gap of 2.7–2.8 eV, while still retaining a low hole effective mass [19]. The intrinsic p-type conductivity in SnO is attributed to Sn vacancies and other acceptor-like defects [20]. Density-functional defect studies show that aliovalent dopants (e.g., group-I or group-V species) can stabilize both p- and n-type regimes in SnO. This bipolar doping behavior is thermodynamically feasible and opens a route for ambipolar transport.

2.2.2. SnO_2 oxygen vacancies and donor defects

Stoichiometric n-type SnO_2, which crystallizes in the rutile structure **(as given in** Fig. S2**),** exhibits conduction originating primarily from shallow donor states associated with oxygen vacancies (V_o) and cation dopants such as F, Cl, or Sb [21]. O 2p states dominate the valence band of SnO_2, whereas the conduction band minimum has strong antibonding character between Sn 5s and O 2p. This electronic configuration results in a low electron effective mass and enhanced electron mobility when defects are properly controlled [22,23]. Defect-engineering studies indicate that oxygen vacancies, Sn interstitials, and surface dangling bonds introduce sub-gap states that enhance conductivity depending on their energy levels and density [24]. These defects also influence band alignment, Fermi-level pinning, and interfacial recombination at perovskite/SnO_2 interfaces. Partial reduction of SnO_2 to SnO_x or the formation of Sn/SnO_2 composite phases can further modify the electronic landscape, affecting charge extraction and transport, and the fundamentals are shown in Fig. 3 [25].

2.2.3. SnO_x thin-film compositions and transport phase diagram

SnO_x transport polarity under sputtering and ALD conditions is observed by growth conditions which control oxygen chemical potential, Sn^{2+}/Sn^{4+} balance, and oxygen-related defects that determine the phase fraction (SnO-like Vs SnO_2 like) and the dominant carrier type. Consider that on fixed oxygen flow, sputtering power controls the energy of deposited atoms and, on re-sputtering, thereby alters the oxidation and defect density, which can result in a shift of film stoichiometry and transport polarity. This was reported in Li et al. work that increasing the sputtering power at a fixed oxygen flow leads to a transition from n-type to p-type conduction, approaching near-intrinsic behavior [26]. For instance, at a constant temperature and deposition method, changing the oxygen availability shifts the balance between SnO-like and SnO_2-like fractions and alters the defect concentration,

leading to a narrow composition window where the transport behavior remains stable, this was illustrated by Barros et al. that p-type SnO_x conduction in low-temperature thin film transistor (TFTs) is stable only within a narrow oxygen partial-pressure window (2.8–3.8%), highlighting the strong coupling between composition, phase fraction, and transport properties [27]. Finally, pointing to low temperature ALD, the oxidant/reactant chemistry and dosing (pulse/exposure) conditions control the Sn oxidation degree and enable tuning them as Sn^{2+}/Sn^{4+} mixed valence**.** Recently, Zhang et al. investigated low-temperature ALD SnO_x and mapped the electrical evolution of the films by tuning the Sn^{2+}/Sn^{4+} ratio [18]. Their results correlate the emergence of hole-transport channels with mixed-valence chemistry, providing a clear chemical basis for the development of ambipolar SnO_x interlayers in perovskite devices.

2.3. Electronic structure of Ambipolar SnO_x

The electronic structure of SnO_x ($1<x<2$) supports its tunable polarity and its unique ability to function as an electron transport layer (ETL), a hole transport layer (HTL), or an ambipolar interlayer in a perovskite solar cell. The Sn–O system creates an electronically rich landscape governed by mixed-valence chemistry, lone-pair activity, and defect-sensitive band alignment. A pictorial energy level alignment is shown in Fig. 4.

2.3.1. Band structure and bandgap characteristics

SnO and SnO_2 occupy opposite extremes of the SnO_x band structure. SnO exhibits a small indirect band gap and a higher optical band gap, arising from its litharge structure. These electronic characteristics arise from Sn^{2+} ($5s^2$) lone-pair interactions, which elevate the valence-band maximum (VBM) and generate strong valence-band dispersion. The highly curved valence band results in a low hole effective mass, promoting efficient hole transport and p-type conductivity [30]. In contrast, SnO_2 exhibits a wide optical band gap of 3.6–4.0 eV and an electronic band gap of approximately 3.0 eV. Its conduction-band minimum is dominated by Sn 5s–O 2p antibonding states, resulting in a low effective electron mass and characteristic n-type behavior. Ambipolar SnO_x occupies an intermediate electronic regime in which Sn^{2+} and Sn^{4+} coexist, resulting in intermediate-band positions and mid-gap transitions. Such behavior is widely observed in ALD- and sputtering-derived SnO_x films used in perovskite photovoltaics [31].

2.3.2. Orbital hybridization and its role in charge transportation

In SnO, the formation of Sn 5s–O 2p antibonding hybridized states produces a strong antibonding character at the VBM. This large dispersion results in a low hole effective mass, high hole mobility, and a shallow VBM, all of which favour p-type conduction. In SnO_2, the valence band is dominated by non-hybridized O 2p states, yielding a deep VBM that is unfavourable for hole transport. Because the conduction band involves Sn 5s states, electron transport is efficient, reinforcing SnO_2 as an n-type semiconductor [32]. In SnO_x, mixed Sn^{2+}/Sn^{4+} valence states form an energetic bridge between the electronic structures of SnO and SnO_2. This mixed-valence environment enables ambipolar transport behavior, allowing SnO_x to support both electron and hole conduction depending on its stoichiometry and defect distribution.

2.3.3. Defect states and mid-gap electronic levels

Mixed-valence SnO_x films exhibit significant defect sensitivity, with mid-gap states arising from Sn^{2+}/Sn^{4+} interfacial disorder, partially filled Sn 5s states in SnO-rich environment, and oxygen defect states are

Table 2
Deposition Technique and its role in Perovskite Solar Cells.

Deposition Techniques	Ref	Sn^{2+}/Sn^{4+} Tendency	Key Control Knobs	Transport Polarity	Scalability Potential	Role in PSC
Reactive magnetron Sputtering	[35]	SnO_2, like Sn^{4+} dominant films, requires highly oxidizing conditions.	O_2/Ar ratio in an oxidizing environment.	n-type SnO_2 ETL behavior	High and industrial compatible	ETL in PSC (n-i-p) structure
	Sputtered SnO_2 ETL by vapor-deposited perovskite [36]	SnO_2 is not as mixed valence	Thinner SnO_2 (~10 nm) is smoother and better crystallised than ~40 nm, shows uniform morphology, and reduced ion migration/ expansion during vapor development.	n-type SnO_2 class ETL behavior	High and demonstrated as a sputtering flexible substrate	ETL in flexible architecture
Atmospheric pressure chemical vapor deposition	[37]	SnO_2 -Sn^{4+} overall valence band spectra	Growth condition (mild vs strong), temperature/ oxidants, time, and thickness optimization	n-type oxide class and SnO_2	Pinhole-free, rapid, no-vacuum, and uniform over 6.25 cm^2	Oxide buffer overlayer in p-i-n stacking
Reactive electron beam evaporation, O_2 partial pressure, and UV ozone	[38]	Sub-stoichiometric on the surface; UV-ozone increases the O/Sn on the surface and widens the bandgap.	O_2 partial pressure during deposition + UV-ozone duration and interfacial oxygen vacancies as trap states.	n-type and ETL behavior	High and compatible substrate	ETL in standard (n-i-p)
Atomic Layer Deposition	[39]	Mixed valence SnO_x with Sn^{4+} and Sn^{2+} in Sn 3d.	Thickness max:7 nm, reduced sputtering and UV damage.	n-type conductivity	Highly positioned-ALD SnO_x for ETL or sputter resistance buffer layers	**Sputter-resistant/ passivation interlayer**
	Low Temperature SnO_x [40]	H_2O-SnO_x results in oxygen deficiency-linked gap states.	Barrier quality/pinhole-free density enables factor for corrosion protection	Electron selective contact/ EEL	High and H_2O-based ALD	Electron extraction layer and permeation barrier
Thermal evaporation under high vacuum	[41]	**SnO/PDTON film show higher Sn^{2+} ratio after ozone treatment compared to SnO (45%)**	Thickness of SnO (40 nm), UV/ O_3 treatment time (20 min), PDTON concentration (0.005 wt%) with spin coating parameters.	Hole transport (p-type)	High scalability for large area 25.2 cm^2 tin perovskite solar cells using SnO/PDTON HTL	Act as HTL, interface, passivation agent, improves hole extraction efficiency, reduces defects, enhances film quality and stability
Electron Beam evaporation	[42]	**SnO phase is process sensitive.**	Substrate temperature, deposition time, film orientation and carrier concentration	p-type	Moderate, vacuum based deposition	Hole transport layer upto 1.16 V

Table 3
Consolidatory comparison on SnO_x as ETL and HTL.

Doped / Undoped	Target Layer Type	Band Gap and Energy Level	Carrier Type and Density Change	Stability Impact	Ref
Undoped SnO_2	ETL and Hole blocking layer	Wide band gap with reduced interfacial recombination (0.10 eV (4.17–4.27 eV) and VBM by 0.06 eV (3.43–3.49 eV). CBM is more negative (deeper)	n-type (intrinsic defects, oxygen vacancies, and Sn interstitials). High electron mobility and low series resistance, Rs = 1.26 Ω cm^2.	Wider bandgap with lower recombination.	[43]
Undoped SnO_2	Electron selective layer (ESL)	CBM is the lower edge and wider bandgap	n-type semiconductor	The device remained stable without encapsulation for 30 days in ambient air.	[44]
Undoped SnO_2	ETL and higher conductivity	Wider band gap with positive conduction band position	n-type or electron-selective behavior. Increased conductivity and high electron mobility	Performance hysteresis was reported with 7.43% PCE and no reported stability	[45]
Nb-doped SnO_2	ETL and rutile structure	-	n-type and increased electron mobility ($2.16 \times 10\text{-}4\ cm^2\ V^{-1}\ S^{-1}$) and trap density 1.74×10^{-15}	Device stored unencapsulated in ambient conditions for 12 days, and PCE was retained 90% after doping	[46]
Undoped SnO_2	ETL or ESL	3.6 eV (SnO_2, typical) / 1.62 eV (perovskite) and Well-aligned CBM/CBM	-	>82% retention after 60h 1-sun MPPT; 20.7% PCE after recovery; >20% after 90 days shelf storage	[47]
Reduced to SnO_x (x < 2)- Mixed valence Sn^{2+} and Sn^{4+} states	Hole Transport Layer (HTL) in inverted Sn-perovskite solar cells	1.4 eV and 3.68 eV for P-SnO_x. Both valence and conduction bands shift upward. The deeper CB, strong p-type.	**p-type**	**P-Nano SnO_x HTL significantly improves device stability and 9.77%**	[48]
Mixed valence Sn^{2+} and Sn^{4+} states (SnO_x)	ETL in planar perovskite solar cells	RT SnO_x eV- 4.12 and SnO_x at 250°C- 3.74. Ec: RT SnO_x = 3.54 and SnO_x at 250 °C = 3.92 Ev 7.66 and 7.62	**n-type for Room temperature produced and n-type with higher carrier density at higher temperature**	Higher Rrec and reduced hysteresis at higher temp	[49]
Mixed valence Sn^{2+} and Sn^{4+} states (SnO_x)	SnO_x amorphous ETL	3.6 eV - SnO_x	**n-type**	15.8 (best), >12 (average, 20 cells), 0.09 cm^2 area, and backward scan	[50]
Mixed valence Sn^{2+} and Sn^{4+} states (SnO_x)	ALD SnO_x on Perovskite (p-i-n)	Not directly measured; affected by impurities and temperature	**n-type**	**Poor device performance when a direct ALD SnO_x/perovskite interface; good when PCBM is used as an interlayer or in an n-i-p structure**	[51]

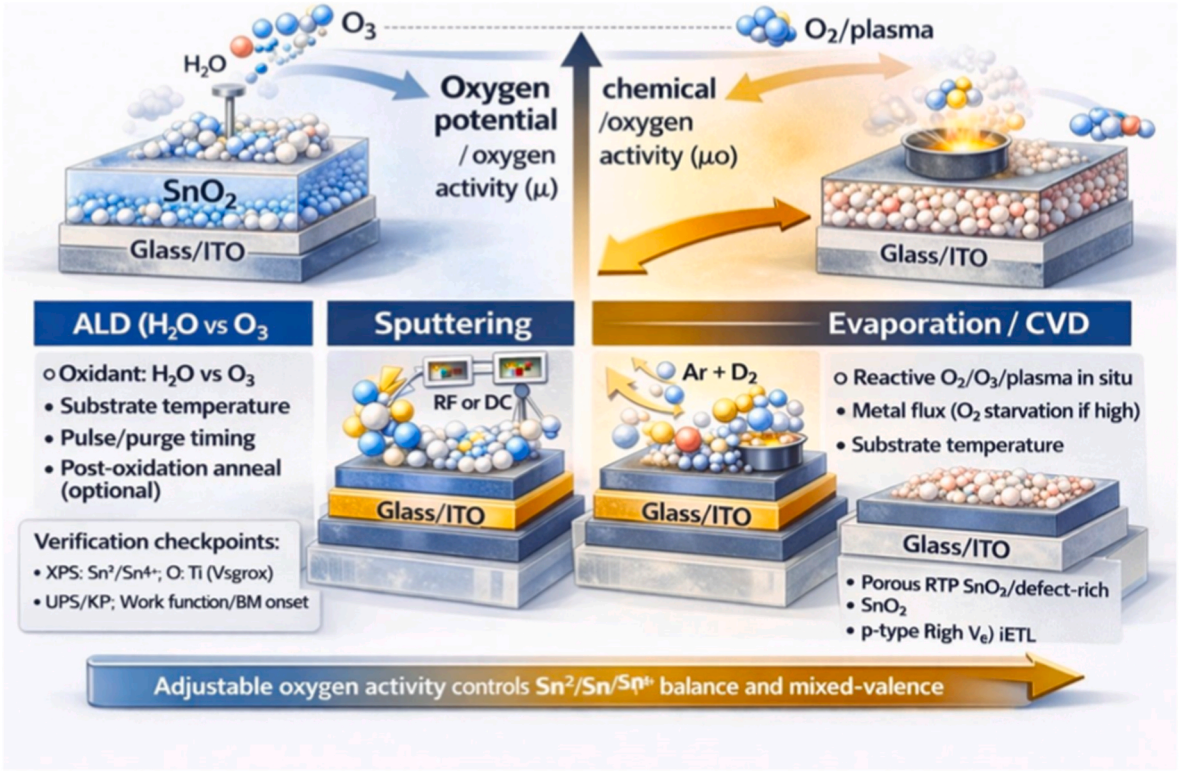

Fig. 5. Schematic illustration of process-controlled SnO_x deposition.

prominent in SnO_2-rich SnO_x. In SnO, p-type conductivity is dependent on acceptor-like defects (V_{Sn}, Sn vacancies), whereas in SnO_2, donor-type defects (oxygen deficiency and/or dopants) have dominant n-type behavior. The overall defect landscape of SnO_x determined by vacancy concentration, valence distribution, and local disorder, ultimately defines whether the material behaves predominantly as a unipolar conductor or exhibits full ambipolar character [33]. Table .1 provides an oversight into primary properties of SnO, SnO_2, and SnO_x

3. Deposition and fabrication strategies for Ambipolar SnOx films

The ambipolar SnO_x layers for perovskite solar cells require a deposition route that controls the Sn^{2+}/Sn^{4+} ratio, oxygen concentration, thickness, and uniformity, while maintaining an interface with the absorber. The SnO_x polarity can be tuned from n-type (ETL) to p-type (HTL) or ambipolar by exploring magnetron sputtering, atomic layer deposition (ALD, including plasma and spatial variants), pulsed laser deposition (PLD), and reactive evaporation/chemical vapor deposition (CVD)-like routes. In addition to vacuum-based techniques, solution-based SnO_x films obtained via sol-gel or ink-based routes provides a low-temperature and scalable depositions, attractive for flexible substrates and large-area device fabrications. These routes resulted in film densification, residual hydroxyl content, and defect distribution via precursor and post-deposition treatments. Based on reported studies, the ETL, HTL, or ambipolar behavior of SnO_x is determined by the valence balance Sn^{2+}/Sn^{4+} and oxygen chemical environment. The deposition method matters indirectly as long as the material composition and defects are controlled [34].

Concern to polarity switch from n-type↔p-type↔near intrinsic in sputtered SnO_x is based on the parameters that can control oxygen chemical potential, phase fraction, compositional balance, and oxygen-related defect population. The significant parameters that impact SnO_x composition and polarity are 1. oxygen partial pressure (O_2 flow), which is the dominant control knob. This can control the oxidation during growth, determine the phase fraction (SnO-like Vs SnO_2-like), and concentration of oxygen vacancies, which results in p-type or stable polarity in a narrow oxygen window. 2. Sputtering power, 3. Pressure, and substrate temperature knobs influences the film densification, scattering, and 4. Reaction kinetics, which impact the defect formation and optical properties of the composition. Also, the post-annealing process can impact the chemical and structural evolution of SnO_x, phase shift, and transport polarity. Some of the reported surveys are given in Table .2 and pictorial illustration in Fig. 5. Across the ALD, PLD, evaporation, and CVD techniques, the SnO_x polarity is also based on O_2 partial pressure, dose, deposition temperature, plasma conditions, and post-annealing atmosphere that aids in tuning the Sn^{2+}/Sn^{4+} ratio and defect density, which shifts the phase fractions and Fermi level position (see Table 3).

3.1. Reactive magnetron sputtering

Reactive radio-frequency (RF)/direct-current (DC) magnetron sputtering from a metallic Sn target using an Ar + O_2 plasma is one of the most promising ways to tune the SnO_x stoichiometry and transport polarity. Han et al. observed that by adjusting oxygen partial pressure during reactive DC sputtering, followed by heat treatment, gives systematic transitions in phase fraction (Sn/SnO/SnO_2) and defect chemistry, enabling access to p-type SnO_x within the specific oxygen/annealing windows [52]. This complements the n→p switching by pointing out that polarity is not only set by the plasma conditions but can be rewritten post-deposition. Watanable et al. found that the sputtered SnO_x initially resulted in n-type behavior and shift to p-type using mild annealing, consistent with structural or chemical evolution towards SnO-rich bonding and acceptor-like defect populations [53]. Also, Jung et al. interpreted that SnO_x films are highly absorbing, with mixed valence SnO rich composition from transparent n-type SnO_2 by correlating the sputtering power, pressure, and substrate temperature with optical gap in the process window [54].

SnO_2-SnO_x electron transport layers are excellent and scalable modules for perovskite solar cells. Qiu and co-workers demonstrated that room-temperature sputtered SnO_2 ETLs can be used to fabricate large-area perovskite modules with excellent long-term operational stability. Their results show that sputtering is already a practical and scalable method for producing Sn-oxide ETLs, even when the films are predominantly n-type [55]. Similar high-performance perovskite modules with sputtered SnO_2 ETLs, results are compatible with a large area glass substrate. Ni et al. demonstrated ambipolar behavior highly relevant to perovskite tandem cells by developing SnO_{2-x} interlayers containing mixed SnO/SnO_2 phases [56]. These mixed-valence films exhibited simultaneous electron and hole transport, enabling their use as a multifunctional recombination layer in all-perovskite tandem architectures. Although their deposition conditions were optimized specifically for tandem stacks, the study clearly shows that reactive sputtering followed by controlled oxidation or reduction can produce SnO_x films capable of functioning as both ETL- and HTL-like interlayers. Jia et al. observed that p-type SnOx will be achieved by reactive magnetron sputtering on a metallic Sn target under controlled non-stoichiometric conditions. The main stabilizing process is the transition region between metallic and oxidized target states, which gives precise control of oxygen incorporation. Under a controlled window, the film shows a SnO dominant with lesser SnO2/Sn3O4 phases resulting in p-type hole transport. They show that the carrier polarity of SnOx is mainly based on oxygen, target surface oxidation state, and phase balance, rather than by extrinsic doping [57]. In contrast, Fortunato et al. discussed that p-type SnOx thin films deposited using reactive rf magnetron sputtering at room temp, and followed with low temperature annealing at 200 °C in air exhibits a clean p-type conductivity after annealing. By tuning the oxygen partial pressure with a narrow growth window, they will show polycrystalline films with α-SnO with minor β-Sn/SnOx phases. The study further shows a p-type transport appears in a limited oxygen pressure regime by highlighting the critical role of stoichiometry control and post-annealing in stabilizing hole-conducting SnO_x [58].

3.2. Atomic layer deposition (thermal, plasma, and spatial ALD)

For ambipolar SnO_x, the ALD technique is the most accurate route, as it results in Å-level controlled thickness and absolute conformality at low temperature. This allows non-dependent tuning of cation valence and oxygen stoichiometry. The traditional thermal or plasma-assisted ALD of SnO_2 using Sn precursor and H_2O/O_2 plasma is widely used for developing low-temperature ETLs (≤80-120 °C) with high efficiency and stability. Erdenebileg et al. have demonstrated that SnO_2 film grown via ALD at 80 °C has efficient ETLs in n-i-p perovskite solar cells. This achieved power conversion efficiency (PCEs) of 18.7% [59]. Kuang et al. grew SnO_2 film via plasma-mediated ALD at 100-200 °C, which showed the layers are capable of providing enhanced interfacial contact and stability compared to TiO_2 ETLs, especially under UV illumination [60]. Hoffmann et al. developed SnO_x at 80 °C via spatial atmospheric pressure ALD as an impermeable electron extraction layer in perovskite cells, which resulted in improved thermal stability and lowered water vapor transmission rate that are essential for long-term device encapsulation [61]. Recently, Gao et al. observed that ALD SnO_x ETLs grown with controlled oxygen vacancies enable perovskite solar cells with remarkable long-term stability [62]. Zhang et al. have used low-temperature ALD to deposit SnO_x film, by tuning the deposition temperature and oxidant conditions, the carrier types can be n-type and p-type. They also suggested that correlating changes in electrical conductivity with changes in the Sn^{2+}/Sn^{4+} ratio and defect monitoring via near-IR absorption can provide adaptable processing conditions for ALD to achieve ambipolar SnO_x [18]. The ALD-grown SnO_x at 80 °C can also act as a multifunctional interlayer in p-i-n type perovskite cell. This makes the

fullerene/perovskite interlayer passivate and enhance the charge extractions [63]. Summing up, these studies show that ALD and spatial ALD enable fine-grained SnO to SnO_2 compositions, and that ambipolar SnO_x ETLs/HTLs are possible by altering deposition temperature, oxidant, plasma conditions, and post-annealing. Gomersall et al. observed p-type SnO can be deposited by atomic layer deposition (ALD) using Sn(II) bis(tert-butoxide) and H2O as the oxidant. They highlighted that ALS is an emerging alternative to conventional sputtering-based routes. This also illustrated that the deposition requires optimization of Sn precursor pulse length, substrate temperature, and multi-phase delivery mode, along with post deposition annealing and Al_2O_3 passivation, which are needed for p-type TFT behavior. It is also noted that using multiple Sn pulses per ALD cycle will improve the crystallinity and device performance than single pulse process. This shows that the precursor dosing is a crucial strategy for p-type SnO stabilization [64].

3.2.1. Pulsed laser deposition (PLD)

Pulsed laser deposition (PLD) gives a stoichiometric transfer from a ceramic target, high purity, and good control of film density. The PLD is a traditional lab-scale technique; a recent report states that it is scaled and engineered for low damage SnO_2/SnO_x ETLs. Zanoni et al. used a widespread PLD tool with a droplet trap to deposit SnO_2 ETLs and studied how the pressure and the oxygen concentration would influence the surface roughness and oxygen vacancy content. The optimized SnO_2 ETL from PLD has resulted in PCEs >18% in n-i-p PSCs. On comparing the ALD SnO_2, the PLD-produced SnO_2 or SnO_x film will produce high-quality ETLs with tunable vacancy concentration [65]. Also, Soltanpoor et al. have produced "low damage scalable PLD" SnO_2, which is suitable for p-i-n type PSCs, with the flexible substrate, controlled laser fluence, and lowered gas, which will minimize the ion bombardment and protect perovskite integrity. The produced devices have obtained efficiency comparable with the ALD-based reference, which states that the PLD-fabricated SnO_2/SnO_x film is compatible with low thermal budget and flexible architecture [66]. The PLD can process independently by controlling the oxygen partial pressure during growth, which can be well applied to grow non-stoichiometric SnO_x with tunable oxygen vacancy profiles. The PLD method can be considered for producing ambipolar SnO_x interlayers and buffer layers.

3.3. Reactive evaporation and chemical vapor deposition (CVD)

Beyond all the previously discussed techniques, reactive e-beam evaporation and CVD processes allows a fine control over the oxygen content and crystal quality of SnO_x layers. Thus, Hossain et al. illustrated that crystalline TiO_x and SnO_x layers were deposited via reactive e-beam evaporation in controlled O_2 pressure along with annealing at 200 °C. They reported that varying oxygen pressure during metal evaporation will control oxide stoichiometry and band positions. This conditioned processed crystalline SnO_x film will significantly enhance the PSC performance by tuning the electron extraction and hole blocking [67]. On the other hand, Yang et al. have examined SnO_x as a buffer layer between ETL/Perovskite and sputter TCOs. This verifies whether the electrical and barrier properties are dependent on deposition conditions and oxidation state. Authors stated that the SnO_x grown under controlled conditions will potentially secure the underlying layers from sputter damage by maintaining good carrier selectivity and band alignment [68]. These vacuum evaporation/CVD-type routes are attractive for ambipolar SnO_x due to the stabilizing factors for mixed Sn^{2+}/Sn^{4+} states and Fermi level position, such as oxygen partial pressure, plasma assistance, and post-annealing.

Saji et al. have illustrated in their review that p-type SnO is predominantly obtained via physical vapor deposition routes such as sputtering, Pulsed laser deposition, and evaporation deposition, which require a narrow process window due to SnO metastability. They showed that oxygen partial pressure, growth temperature, and deposition rate are critical in determining whether a pure-phase SnO film or a mixed $Sn/SnO/SnO_2$ film is obtained. Also, their review further shows that the metallic Sn, SnO_2, and mixed phase targets have been used, while post deposition oxidation and disproportionation remain the key challenges for phase stability. Thus, the fabrication of p-type SnO depends on perfect stoichiometry and process control to stabilize the hole-conducting SnO phase [69].

3.4. Ambipolar SnO_x interlayers in tandem architecture

The techniques described above focus on n-type ETLs; ambipolar SnO_x has been widely used as a recombination and interconnecting layer in tandem. Palmstrom et al. developed SnO_x-based inorganic recombination layers in flexible perovskite tandems, combining vacuum-deposited oxides with organics and perovskite subcells. Their study found that well-engineered SnO_x layers can provide sufficient conductivity for electron-hole recombination while remaining optically thin and mechanically durable [10]. Xiu et al. stated that highly efficient perovskite-organic layered solar cells, which use a simple ambipolar SnO_x interconnecting layer, facilitate the recombination of electrons and holes from the two cells, ultimately reducing voltage loss and phase segregation. This demonstrates that controlling the stoichiometry and defect states of vacuum-processed SnO_x allows it to function as a true ambipolar transport layer rather than purely an electron-selective ETL [70]. This supports that SnO_x grown under controlled vacuum-deposited SnO_x can yield ambipolar transport and intermediate concentrations.

4. Validating SnO_x as the electron transport layer (ETL) in n-i-p perovskite solar cells

In n–i–p perovskite solar cells, the electron transport layer (ETL) controls the electron extraction, hole blocking, interfacial recombination, and operational stability. Among inorganic ETLs, tin oxide (SnO_x, typically SnO_2-rich) has emerged as an ideal choice. The SnO_x is found as an efficient replacement for TiO_2 in high-efficiency planar architecture. Recent reports state that SnO_2-based ETLs are efficient and stable n-i-p devices, due to their combined advantages of wide bandgap (high transparency), high electron mobility, perfect band alignment with lead halide perovskites, and closeness with low-temperature processing routes [71]. Below are the factors that make the SnO_x more beneficial than the conventional TiO_2 ETL layer.

4.1. Energy level alignment and charge selectivity

The SnO_x ETLs function well due to their adjustable band alignment with iodide-rich perovskites, such as $MAPbI_3$, $FAPbI_3$, or mixed halides. These kinds of perovskite have CBM around −3.9 to 4.1eV, whereas the SnO_2 and oxygen-rich SnO_x films generally provide CBM of −4.3 to −4.5 eV, which is slightly lower than the perovskite CBM. This energy offset can result in a downhill pathway for electron extraction from perovskite to SnO_x, making them an ideal choice for ETLs in n-i-p PSCs. Additionally, SnO_2 blocks the holes due to its deeper valence band, and fewer defects that lower the traps and recombination at the interfaces. Chen et al. summarized that SnO_2 offers a higher electron mobility and a more adaptable CB alignment for electron extraction than TiO_2, and that its valence band blocks holes and reduces interfacial recombination [72]. Furthermore, Park and Zhu observed that when interface traps are made unreactive, SnO_2 ETLs can achieve high open-circuit voltages and reduced hysteresis in planar n-i-p cells. This demonstrates that SnO_2 has an intrinsically well-aligned band structure for improved charge extraction from the perovskite absorber [73]. These energy level considerations are closely related to the ambipolar SnO_x design. As the Sn^{2+}/Sn^{4+} ratio and oxygen-vacancy concentration are adjusted, the positions of the CBM, VBM, and mid-gap states shift accordingly. These changes allow SnO_x to evolve from a highly electron-selective ETL-like material to one that supports more balanced, ambipolar charge transport. Thus, the SnO_2-rich SnO_x has favourable CB alignment for electron

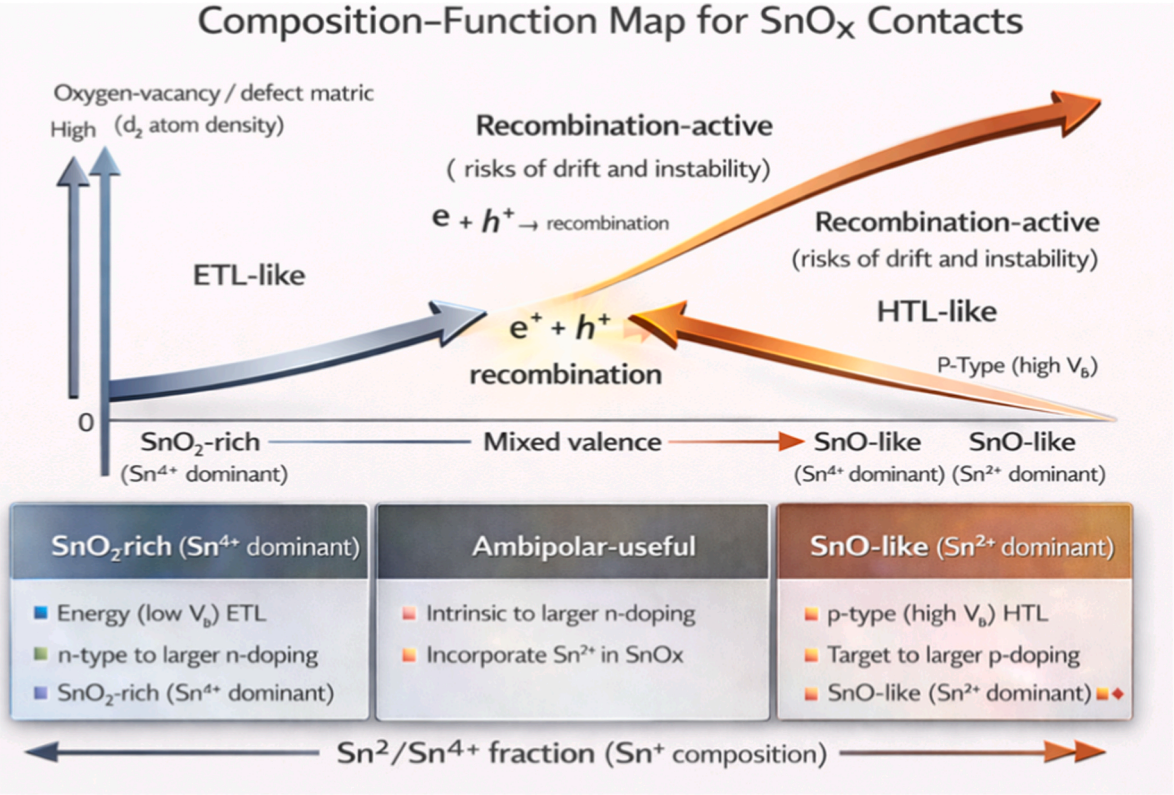

Fig. 6. Composition–function map for SnO_x contacts in perovskite solar cells, relating the Sn^{2+}/Sn^{4+} composition and defect density to SnO_x functionality, transition from n-type, p-type films through mixed ambipolar regime.

extraction and deep VB for hole blocking. Tuning Sn^{2+}/Sn^{4+} and oxygen vacancy concentration shifts CBM/VBM and gap states, which result in SnO_x rich in ETL or more ambipolar transport.

4.2. *Defect and doping engineering of SnO_x ETLs*

Essentially, SnO_2 is n-type; its ETL properties depend on carrier density, oxygen vacancies, and dopants. Controlling its n-type nature can enhance conductivity and lower series resistance. Increased oxygen deficiency creates deep defects that can reduce Voc and stability. A more detailed review by Hoang et al. shows that aliovalent cation doping (e.g., Zr, F, Cl, KF, SbF_3, Mg, and Nb) can adjust the carrier concentration, mobility, and band positions of SnO_2 while maintaining high transparency [74]. Meanwhile, Tian et al. developed Zr/F co-doped SnO_2 (Zr/F: SnO_2) ETLs at temperatures $\leq$150 °C, showing higher conductivity, fewer defects, and better band alignment with perovskite. This resulted in planar n-i-p PSCs with PCEs over 20% and significantly reduced hysteresis [75]. Similarly, Eliwi et al. improved nanostructured SnO_2 ETLs for planar n-i-p cells by combining compact and nanoparticulate layers. Modifying the ETL structure revealed that a bilayer arrangement can improve electron extraction and lower J-V hysteresis [76]. Therefore, these defect and doping studies demonstrate that the Fermi level and CBM/VBM can be tuned by carefully adjusting vacancies and dopants. As the Sn^{2+} fraction and oxygen deficiency increase beyond the strongly SnO_2-rich regime, these factors serve as adjustable controls that gradually shift SnO_x toward more ambipolar transport, maintaining sufficient electron selectivity for stable ETL operation. SnO_2 is generally n-type, and its defects, like oxygen vacancies, can strongly affect the conductivity, $V_{oc,}$ and stability. Thus, the doping and co-doping can help in adjusting the carrier density, energy levels, and lower the defect-related losses by retaining the film transparency.

4.3. *ETL stacking, interfacial engineering, and nano-structuring strategies*

Despite single-layer compact SnO_2, the stacked or nanostructured ETLs are highly used in high-performance n-i-p devices and are considered interfacial engineering for reducing recombination and enhancing stability. Zou et al. have fabricated low-temperature UV-Ozone sintering for ZnO/SnO_2 bilayer ETLs. The ZnO underlayer is encapsulated by UV-treated SnO_2 film. The dual-layered structure combines the high mobility of ZnO with the deep valence band and chemical robustness of SnO_2, enhancing improved electron extraction, open-circuit voltage, and better stability compared with single-layer SnO_2 [77]. SnO_2 nanostructure has also been explored by Zhang et al. who observed that SnO_2 nanorod arrays with controlled area density will function as efficient ETLs, resulting in enlarged interfacial area for charge extraction without recombination [78]. In brief, Park and Zhu, and Chen et al. a wide range of surface-treatment and passivation strategies such as halide-based treatments, small-molecule modifiers, and self-assembled monolayers are routinely applied to SnO_2 ETLs to reduce interfacial trap densities, tune surface energetics, and promote high-quality perovskite crystallization [72,73]. These same approaches can be directly applied to SnO_x films that are intentionally oxygen-deficient or mixed-valence, ensuring that even ambipolar SnO_x compositions can be engineered to remain sufficiently electron-selective for ETL operation. In brief Bu et al. reported the universal potassium interfacial passivation strategy produced out of slot-die printed tin oxide (SnO_2) ETL that achieves high-efficiency, hysteresis-free flexible PSC. The hysteresis will be suppressed by potassium ions at the interface of SnO_2 and perovskite layers. This strategy achieved them with hysteresis-free rigid PSCs with PCE of 20.50% (reverse scan) and 20.46% (forward scan). The passivated device showed excellent light and long-term stability with lower than 5% efficiency loss. Also, it promoted

the grain growth and passivated the interface, leading to lowered trap density, carrier density, and improved charge collection as shown in Fig. S3. Thus, the universal interfacial passivation strategy can offer a potential route for developing high-performance, stable, and hysteresis-free flexible PSCs [79].

The SnO_2-dominant end of the SnO_x spectrum inherently offers strong electron selectivity in n–i–p PSCs because of its deep valence band, favourable conduction-band alignment, and low density of mid-gap states. The systematic introduction of ambipolar behavior can be achieved by increasing the Sn^{2+} fraction and adjusting oxygen-vacancy levels, which shift the CBM/VBM positions and alter the defect state distribution. Throughout this compositional adjustment, established interfacial and defect-passivation strategies originally optimized for SnO_2 remain fully applicable, ensuring that even mixed-valence or oxygen-deficient SnO_x films can be engineered to maintain sufficient electron preference when ETL functionality is needed [80]. In contrast, the presence of a lower valence state in the SnO_x can present a few defects, such as the film might produce with high-density oxygen vacancies and uncoordinated Sn atoms. Also, SnO-rich ends in SnO_x can cause charge trapping, which can result in a non-radiative recombination at the ETL/Perovskite layer, eventually increasing the contact resistance and reducing the open circuit voltage. In addition, the SnO can also result in unfavourable energy level alignment within the perovskite layer, which has an energy barrier for electron transportation. This obstructs the efficient carrier extraction and results in charge accumulation at the interface. If the defect sites are prone to absorbing water, this can lead to degradation of the perovskite and reduce the long-term stability [81]. Thus, the stacked or bilayer and nano SnO_2 ETLs are reported to increase the charge extraction and lower the recombination. Also, passivation suppresses the interfacial traps and hysteresis.

5. Validating SnO_x as the hole transport layer (HTL) in p-i-n perovskite solar cells

In p-i-n perovskite solar cells, the deposition of the hole transport layer (HTL) on transparent conductive oxide (TCO) allows for hole extraction, electron blocking, interface recombination, perovskite nucleation or crystallization, and operational stability. In contrast, conventional organic HTLs (e.g., PEDOT: PSS, poly(triarylamine), which are processed simply, can lead to chemical instability and hidden interfacial losses. These traditional HTLs can also cause issues like interfacial degradation and faster device aging. Due to their resistance to moisture, UV light, and oxygen, they provide weaker diffusion barriers. To address these drawbacks, an inorganic alternative is needed [82,83]. Therefore, SnO_x ($1 < x < 2$) can be used as an HTL when it exists in SnO or mixed valence (Sn^{2+}/Sn^{4+}) regimes, enabling p-type or ambipolar transport and tunable valence band positions. Over SnO_x, a SnO_2-rich oxide acts as an electron-selective layer in p-i-n architecture, Fig. S4 shows the energy and photoelectronic measurement of Sn-based PSC and PEDOT: PSS [84]. The significance of SnO_x as a p-type material is also reported by a few researchers in various applications, Lv et al., who have reported an article based on the radiation stability of the p-Type SnO_x TFT with Al_2O_3 and HfO_2 passivation layers. This validates the SnO_x as a promising p-type semiconductor suitable for HTL in TFTs. They have passivated Al_2O_3 to enhance the SnO_x device stability and radiation tolerance, which makes them a suitable choice for applications in radiation-prone environments like space or nuclear fields. Their report provided insight for improving the SnO_x device reliability via proper passivation [85]. On the other hand, via hydrogen plasma treatment and Al doping on SnO_x film shows stable p-type conductivity, enhances mobility, and carrier transport was reported by Pan et al. This demonstrated a strong electrical performance with a threshold voltage of about −5.2V and an on/off current ratio (Ion/Ioff) of 10^5. Also, the subthreshold swing (SS) slightly increases with doping but shows a range of (183.6 mV/dec). The theoretical analysis, such as DFT, resulted in Al doping having widened the bandgap (0.013 eV to 0.237 eV) and lowering the hole effective mass [86].

5.1. Energy-level alignment and hole selectivity

To work efficiently, the hidden interface contact produces low-barrier hole extraction and electron blocking selectivity, suppressing interfacial nonradiative recombination. In SnO/SnO_x, the SnO is a rare p-type oxide with dispersive valence state and critical contact design (work function, which can be high depending on surface termination and growth conditions). The SnO has work function values ranging from 4.3eV to >5 eV. DFT reports show an average value of around 5.8 eV, with an experimental value of 5.2 eV, collectively highlighting strong tunability [87]. The device-level validation of SnO as HTL has illustrated that SnO thin films can work as HTL in PSC. SnO/SnO_x can result in hole contact in p-i-n PSCs due to its p-type oxide and tunable work function, which allows low-barrier hole extraction and electron blocking with designed interfaces.

5.2. Low-temperature SnO_x HTLs for planar p-i-n architecture

A practical advantage of SnO_x as an HTL source is compatible with low thermal budgets, which is crucial for HTL as it has a buried interface layer and remains favourable with a TCO substrate, subsequent perovskite deposition, and a flexible temperature-sensitive route. The thin film engineering shows that low temperature growth of ambipolar SnO_2 can be a transportation layer or interconnection layers in perovskite devices [88]. In addition, the plasma-mediated processing has been used to prepare a SnO_x layer that works as a bottom HTL in inverted tin-based perovskite stacks, which shows that low temperature, scalable surface control can yield HTL-relevant SnO_x [89].

5.3. Defect and doping engineering to induce p-type /ambipolar transport while suppressing recombination

The SnO_2-rich SnO_x (n-type), SnO_x acting as HTL needs acceptor-type conduction and minimal trap-assisted recombination at the hidden interface. This refers to controlling the Sn^{2+}/Sn^{4+} ratio (Stabilizes the bonding without SnO_2 oxidation), cation/oxygen vacancy balance, and dopant/alloy strategies, which improve the hole mobility and stabilize the p-type condition. The recent work details the target of p-type SnO_x ($x < 2$) and observes that the incorporation of elements like Ge can boost the hole mobility, which benefits in low series resistance and higher fill factor (FF), reducing interfacial charge accumulation and nanoradiative recombination [90]. Computational studies (DFT and band-alignment analysis) show that SnO-based SnO_x can achieve a sufficiently high work function, which is required for efficient hole extraction and electron blocking. Therefore, controlling defects and employing alloying and dopant engineering are essential to ensure that SnOx consistently behaves as a reliable HTL.

5.4. HTL stacking, buried interface engineering, and crystallization control

In p-i-n devices, the hidden HTL or perovskite interface is often the dominant loss channel due to nucleation, defect formation, and interfacial recombination. In brief, buried HTLs (e.g., via nanoparticle homogenization, interface passivation, and energetics control) are important to unlock the high fill factors and stability [91]. The SnO_x--based HTLS, with control over its surface chemistry or growth process (plasma, ozone, chemical treatments), tunes its function and wettability to promote uniform perovskite growth. The bilayers or stacked HTLs act as basic HTLs or passivated interlayers, which, on pairing with high

Table 4
Stability metrics and PCE of various SnO_2-based PSC.

Type	Processing Technique	Perovskite composition	Test Condition	Stability Test Type	Retention	Voc (V)	Best PCE	Ref
SnO_2	ALD @ 200 °C with a thickness of 15 nm	$FAMAPb(IBr)_3$	Thermal Treatment for 24h at various temp.	Heat stability of SnO_2 film (sheet resistance change)	Sheet resistance <9% after heat treatment	0.93	15%	[108]
SnO_2 @ various temp = 180 °C, 300 °C and as deposited	ALD@80 °C with 5-15 nm thickness	Methylammonium lead iodide ($MAPbI_3$)	-	Thermal stability analysis of SnO_2 film		1.07-SnO_2 @180 °C	18.3%- SnO_2 @180 °C	[109]
SnO_2 nanocrystal and Flexible SnO_2 substrate	Low temp wet chemical sol gel (reflux:40 °C); Spin coating and UV-Ozone treatment	$(FA_{0.85}MA_{0.15})Pb(I_{0.85}Br_{0.15})_3$	UV illumination and with N- filled chamber with AM-1.5G without UV and MPP over 50 h	UV and operational stability.	96.3% retained after 100min UV and 60% after 50 h	1.17V	19.20%	[110]
Mesoporous-SnO_2 (m-SnO_2)	Spin coating of SnO_2@ high temp 450 °C, spray pyrolysis of SnO_2	$Cs_{0.05}(FA_{0.79}MA_{0.16})Pb(I_{0.83}Br_{0.17})_3$	1.5 a.m. solar light (100 mW/cm^2) MPP tracked for 10h at N-atmosphere.	UV and operational stability	End-of-test PCE (t = 10 h): m-TiO_2 13.0, planar SnO_2 15.6, m-SnO_2 10.4	0.98 on AZO and 0.94 on FTO	13.1% on AZO and 11.4% on F5TO	[111]
PAA-SnO_2	Slot die printing of SnO_2 nanocrystal inks	**$FAPbI_3$:MACl**	Storage at ambient conditions for 1000h and also for 85 °C. continuous 1-sun illumination, MPPT for 500h	**Storage capacity at ambient, thermal aging @ 85°C, operational stability via light soaking (unencapsulated), and flexibility check**	Retained 80-95% on average for every time, various, and 86% PCE after 2000 bending cycle	1.18	22.5% and 16.4% for 30 × 30 cm^2	[112]
Bilayer SnO_2	Bottom-ALD SnO_2 and Top-Sol-gel SnO_2	α-$FAPbI_3$	N_2 environment at 20% humidity for 1300h	Storage stability	85% efficiency after 1300 h	1.15	23.86%	[113]
ZnO-SnO_2 bilayer	ALD: SnO_2 (17 nm) on ZnO (28 nm) @ 120 °C and annealed @ 200 °C for 30Min.	$Cs_{0.05}FA_{0.8}MA_{0.15}Pb(I_{0.75}Br_{0.25})_3$	-	-	-	1.23	18.1%	[114]
NH4Cl coagulated SnO_2	Spin coating and modified 50 mM NH4Cl and annealed @ 60 °C	**Mixed cation-$FA_{0.95}MA_{0.05}PbI_3$**	AM 1.5 G illumination, MPPT and duration explicitly.	Operational stability (MPPT and unencapsulated)	SnO_2-78% after 1500h and NH_4Cl-SnO_2 reatined 90%	1.15	21.3%	[115]
SnO_2 dots	Colloidal SnO_2: Spin coating	$Cs_{0.05}(MA_{0.17}FA_{0.83})_{0.95}Pb(I_{0.83}Br_{0.17})_3$: Triple cation with mixed halide	-	-	-	1.13	20.79%	[116]

mobility HTLs, can reduce contact resistance by retaining the chemical robustness [92,93].

6. Doping, alloying, and interface passivation for enhancing electronic structure control in SnO_x

Doping, alloying, and interface engineering are considered significant processes for converting "baseline" n-type SnO_2-rich films into electronically structured and partially reduced SnO_x layers that can operate as high-end ETLs, HTLs, or ambipolar interlayers. These approaches can work by shifting the conduction and valence band edges, controlling carrier polarity and density via oxygen vacancy and Sn^{2+}/Sn^{4+} balance, and suppressing non-radiative recombination at buried interfaces.

6.1. Aliovalent, doping, and alloying to tune band structure and ETL energetics

SnO_x ETLs with SnO_2, aliovalent cations, and anion dopants are widely used to modulate band-edge positions and carrier density while maintaining high transparency. In recent reports, the Cerium (Ce) doping by Ahmmed et al. onto the colloidal SnO_2 ETLs showed a Ce^{3+}/Ce^{4+} redox couple. This can passivate the surface defects and upshifts the SnO_2 CBM close to the perovskite absorber, that resulted with the Voc loss associated with an overly deep CBM and reduced surface oxygen vacancy. The PCE was increased from 21.1% to 23.0% after doping Ce onto SnO_2 at 100 mV, having improved Voc and lowered hysteresis. In addition, 2D phenethylammonium iodide was capped as a layer, which produced a Voc of 1.19 V and PCE of 23.3% are achieved on 0.09 cm^2 devices, as shown in Fig. S5 [94]. On the other hand, halide-related alloying provides another perspective on band alignment and defect chemistry. Zhang et al. used potassium fluoride (KF) to introduce K^+/F^- at the ETL surface, eliminate -OH-related deep traps, and lightly raise the effective CBM. This reduced interfacial recombination and enhanced Voc from 1.18 to 1.31 V, with PCE raised from 13.40% to 15.39% in FTO/ SnO_2/KF/$CsPbI_2Br$/ carbon devices [95].

Transition metal or main group dopants can be adjusted to control the electron density and mobility. Ye et al. doped Zinc (Zn) onto SnO_2 as a low-temperature ETL in carbon-based planar PSCs, using Zn^{2+} to modify the carrier concentration and film morphology. This resulted in

PCEs of up to 17.78%, significantly higher than the SnO_2 control, which maintained high optical transparency [96]. Theoretical work by Sannino et al. explained that Mg^{2+} doping in SnO_2 caused an upward shift in CBM and reduced intra-gap states, potentially controlling Mg with an improved CBM by 0.1-0.2 eV and Voc [97]. These aliovalent doping and alloying strategies are applied to ambipolar SnO_x by controlling Sn^{2+} through average cation/anion doping. This adjusts the CBM (ETL functions), VBM, and Fermi level (HTL functions), by reducing defects, and the Fermi level can be blocked despite the doping techniques.

6.2. Enabling p-type and ambipolar behavior in SnO_x

The ambipolar SnO_x films needed a shift from the conduction band side (n-type) to mid gap or even close towards the VBM (p-type), without affecting the transparency or mobility. Basic defect chemistry analysis by Scanlon and Watson illustrated that by incorporating acceptor dopants (eg., Mg^{2+}, Zn^{2+}, and In^{3+}) without any loss of oxygen vacancies, and perfect growth conditions can significantly stabilize the acceptor defects [98]. He et al. realised that Mg^{2+} substituting for Sn^{4+} creates an acceptor level which drives the Fermi level to VBM, resulting in a hole concentration of 10^{17}-$10^{18}\,cm^{-3}$ at room temperature with hole mobility of a few $cm^2V^{-1}S^{-1}$ [99]. Later, Fu et al. have achieved wide bandgap p-type SnO_2 via two step oxidation/reduction process, which obtains a reproducible p-type conductivity (hole concentration $\approx 2 \times 10^{18}\,cm^{-3}$) and Fermi level positioned within 0.2 eV of VBM with bandgap of $\geq$3.5 eV [100]. As these studies are not yet combined with PSCs device stacking, these reports provide a scientific insight for using Mg or In-doped SnO_x as HTL or ambipolar layer in p-i-n devices. Mainly, the SnO_2-rich composition can be combined with SnO_x-rich ambipolar phases, which result in SnO/SnO_{2-x} stacks. Such stacks are structured with SnO_2 (n-type) for electron extraction and the perovskite region with a high fraction of Sn^{2+}, providing them with a shallower VBM and efficient hole extraction, resulting in an electronically ambipolar SnO_x layer. Fig. 6 illustrates the compositional map for SnO_x in PSCs.

6.3. Interface engineering and defect passivation at SnO_x/ perovskite contacts

On desired SnO_x composition, the hidden interface losses can dominate. The interface engineering (molecular modifier, 2D interlayers, and ultrathin oxides) is essential for reducing band offsets and non-radiative recombination, which can result in an intrinsic ambipolarity of SnO_x. When Yang et al. produced E-SnO_2 ETL by complexing SnO_2 colloids with EDTA, they resulted in a higher work function, enhanced electron mobility, and lowered surface traps. Using E-SnO_2 in planar PSCs, E-SnO_2 will achieve PCEs of 21.5-21.6% and reduced VoC decay and negligible hysteresis due to concealed interfacial recombination with an excellent mobility matching with the HTL [101]. Additionally, an ultrathin ALD passivation layer will provide a high degree of freedom. Zhang et al. have reported an ITO/SnO_2 interface using sub-nanometered Al_2O_3 grown by ALD to passivate the defect that acts as a recombination centre, the devices will exhibit the higher VoC and fill factor, and PCEs >21%, by maintaining good electron extraction through tunnelling [102]. All the above concepts justify that ambipolar SnO_x layers can be used as the HTL side contact in p-i-n cells. For example, the SnO rich with a slight p-type and SnO_x with a 2D perovskite capping layer at the perovskite/HTL interface will shift the interfacial Fermi level towards the VBM and block electron back injection. Sutanto et al. and Zhong et al. have reported that the 2D/3D perovskite heterostructures will reduce the non-radiative loss that will dominate in losing VoC from the bulk perovskite. The mixed Sn-Pb devices having both ETL and HTL interfaces are equally passivated. Also, the typical phosphonic and carboxylic acid-tuned metal oxides will function at 0.2-0.4eV, with 50-150 mV of improved Voc when the shift reduces the interfacial band bending and suppresses recombination [103,104]. From the above studies and discussion, it is understood that the SnO_x layer has the potential to act as an efficient ETL and HTL by combining bulk doping/alloying (Ce, Mg, Zn, Halides, etc.) with perfect interface modifiers (SAMS, 2D perovskites, and ALD oxides), whose CBM and VBM will be independently structured to perovskite bands.

7. Stability, degradation mechanisms, and reliability of Ambipolar SnO_x contacts in PSCs

7.1. ETL-mode SnO_2-Rich SnO_x (electron-selective)

SnO_2-rich SnO_x is typically robust and UV-tolerant relative to many other oxides, but its durability is highly dependent on interfacial defect chemistry. Also, the dense film formation can physically prevent the contact of moisture or air, and control the surface defect landscape [105]. The high oxygen vacancy (Vo) populations produce a reactive/adsorptive site that results in iodide diffusion and accelerates FAI deprotonation (Formamidinium iodide), which raises the interfacial nonradiative loss and long-term drift. As a complementary durability lever, the high-density ALD SnO_2 in a dual-layer ETL has been reported to inhibit vertical ion migration, which can increase the thermal durability (e.g., 85 °C/10% RH for 1000h) relative to fullerene-based ETL stacks [106]. A commonly reported device-level stability or degradation failure in p-i-n can be prevented by SnO_2 as a barrier layer design (electrode-ion diffusion (e.g., Ag+) into ETL stack), which can stop ion diffusion at thermal aging [107]. Table .4 Provided the PCE and stability matrices of various SnO_2

7.2. HTL-mode SnO_x (SnO-like/mixed valence hole selective)

When SnO_x is rich with Sn^{2+}, the system can provide a high work function, hole-selective contact without the acidity/hygroscopicity penalties of some organic HTLs. Also, the key intrinsic failure mode is $Sn^{2+} \rightarrow Sn^{4+}$ oxidation under wet conditions, which can slowly change the SnO to SnO_2 character (hole selective to electron selective contact) by change in conductivity and band alignment. This Sn^{2+} rich film has controlling factors such as oxygen exposure and oxygen diffusion, as SnO (Sn^{2+} rich film) can easily oxidize to Sn^{4+} under an aggressive aqueous medium [117]. Secondly, there will be a partial oxidation that results in a SnO-SnO_2 p-n junction, which can introduce internal band bending and resistive loss that end up in fill factor loss and contact limit extraction [118]. Practically, the solution-processed SnO_x as HTL in the perovskite solar cell device has shown 90% retention efficiency after 1000h of maximum power point tracking, which was observed that SnO_x as stability improving alternative to PEDOT: PSS, as shown in Fig. S6 [119].

7.3. Ambipolar or interlayer SnO_x (interconnecting or recombination type layer)

When SnO_x is used as an ambipolar interlayer (e.g., in tandem or as multifunctional interfacial layers), it must balance carrier transport and recombination, have low parasitic adsorption, and be chemically robust against solvent or ion diffusion and electron-ion migration to prevent midgap-assisted recombination losses [120]. In perovskite-organic cells, the simple ambipolar SnO_x layer can reduce phase separation and voltage loss, enabling high-performance layers with both electronic and chemical stabilization [121]. Generally, the interconnecting layer highlights that performance and stability are sensitive to layer tuning, Fig. S7 shows device performance of PSC tandem cells.

8. Performance and commercial outlook

Currently, SnO_x contacts are not only “supporting layers” but also valuable levers for improving efficiency and stability compared to certification, operational tracking, and process windows. SnO_2-rich SnO_x is the leading high-PCE endpoint due to its strong hole blocking and defect

Table 5
Industrial approach, Peak PCE of Several Reports on SnO_x.

Cell/module	SnO_x Role	Active Area	Deposition Scalability	Peak PCE %	Stress Condition	Industrial Approach	Ref
FTO/bi-TiO_2/mp-TiO2/ Perovskite/ Spiro-OMeTAD/ Au, FTO/bi-SnO_2/mp-SnO_2/ Perovskite/ Spiro-OMETAD/ AU, FTO/NiOx/ Perovskite/ PCBM/AU)	m-SnO_2 as ETL in n-i-p structure	0.916 cm^2 for encapsulated inverted device (FTO/NiOx/ perovskite/ PCBM/AU)	Paste based Spin coating for m-SnO_2		High-intensity UV (365 nm, 60 mW/cm^2, ~13 × AM1.5 UV intensity); also 1 sun AM1.5G (100 mW/cm^2); tests in N_2-filled glovebox (inert) and ambient (40% RH)	UV-stable ETL/ perovskite interfaces, highlighting PCBM as a promising ETL for durable	[126]
Single-junction p-i-n PSC & 2-terminal all-perovskite tandem solar cells	ETL & internal barrier	**0.06 cm^2** (for single cell testing); larger area in tandem modules	ALD within or ex-situ ozone nucleation; flexible with roll-to-roll & spatial ALD for large scale	24.2	Operational stability tested at 65 °C, 1-sun illumination, N_2 atmosphere, quasi-MPP (ISOS-L2-2I) for 1000 h; additional solvent, thermal, and ambient aging stress tests	High-yield, durable, efficient PSC and tandem modules for commercial use.	[127]
Single junction PSC as n-i-p structure	ETL and coherent interlayer (Cl-bonded SnO_2)	Not stated	Solution processing spin coating, and chemical bath deposition	RS-25.8 & FS-25.6	ISOS-L-1I protocol: unencapsulated device, 1 Sun illumination (AM 1.5G, 100 mW/cm^2, xenon lamp), ambient/inert, 500 h, no UV cutoff	Defect-minimizing scalable interface strategy for highly efficient stable PSCs.	[128]
Single junction PSC as n-i-p structure	ETL deposited as SnO_x via reactive electron-beam evaporation (r-SnO_x)	5 mm^2 (lab-scale device, up to 16–25 mm^2 tested for larger-area pixels	Highly scalable; low-temperature reactive electron-beam evaporation is compatible with roll-to-roll processing, flexible substrates,	19.3	Unencapsulated devices, continuous illumination in air (AM 1.5, 160 h); also, dark storage in N_2 (12 days)	Potential for commercial use as a rapid, low-cost & temp, and roll-to-roll compatible process for SnO_x ETLs.	[129]
Single-junction as p-i-n PSC	Electron extraction interlayer (ALD SnO_x), inserted between C60 ETL and carbon cathode to enable efficient electron collection (polarity inversion)	0.1 cm^2 for carbon-PSC; 0.06 cm^2 for Ag-PSC	ALD SnO_x is process-agnostic: conventional ALD for lab, but compatible with high-throughput spatial ALD and roll-to-roll printing for industry; carbon cathode is solution-printed (scalable)	21.8-C, 24- Ag, & 24.5- BCP/ Ag	Accelerated ISOS-L-2I protocol: N_2 atmosphere, 1-sun equivalent illumination, 45–105 °C, MPP tracking; lifetime projections at 30 °C	3 × lifetime improvement and 60% lower BOM cost over Ag reference; establishes a scalable design rule for durable, low-cost, industrial perovskite PVs.	[130]
Single-junction as p-i-n PSC	P-SnO_x (plasma-assisted SnO_x)-bottom HTL & T-SnO_x as top in situ protection (ETL), reducing Sn^{4+} to Sn^{2+} and decreasing trap density	Not stated	Plasma-assisted in situ deposition- suited for scalable, industrial roll-to-roll processes; perovskite and C60 layers are solution-processed/spin-coated	14.0-P-SnO_x as HTL & T-SnO_x- 13.5 ± 0.32%	Long-term storage: Maintained initial performance for 50 days under N_2 (unencapsulated); operational MPP stability test under 1 Sun illumination for at least 100 s	scalable, low-cost, inorganic HTL/ETL approach for lead-free PSCs, replacing unstable PEDOT: PSS and providing robust in situ protection	[131]
Single-junction as p-i-n PSC	HTL	Not stated	Spin-coating at low temperature (100 °C anneal); compatible with scalable, solution-based, low-cost manufacturing	11.11	Encapsulated device, MPPT under continuous illumination for 1000 h; 90% efficiency; thermal stability (85 °C, 72 h).	stable, low-cost, solution-processable HTM PSCs, overcoming PEDOT: PSS instability and enabling higher long-term stability	[132]

landscape tuning through surface capping, passivation, and band-offset shaping, rather than bulk transport optimization. In 2025, inorganic La-capping on SnO_2 creates an interfacial conduction-band spike, reduces buried-interface strain, and maintains over 80% efficiency after 800 h of continuous illumination, resulting in 26.2% PCE and 25.6% certified efficiency. This positions SnO_x ETL progress as "recombination/strain management at the junction," not "electron mobility in the junction" [122]. The commercial distinction depends on whether the same SnO_x chemistry can be applied uniformly and withstand stress testing, where factors like thickness control, lateral electronic homogeneity, and defect moderation influence yield and drift. A study by Lee et al., suggests ultrathin, oxygen-deficient SnO_x interlayers as a feasible method for "cell-to-module translation" because they can smooth local energy disturbances at the TCO/oxide/perovskite interface and maintain low thermal budgets. Using plasma-modified ALD SnO_x, module PCE increased from 17.9% to 20.1% on a 23.2 cm^2 active area, with 92% retention after 2700 h at 85 °C/85% RH and 96% retention after 1000 h under MPPT, supporting the idea that SnO_x layers can be designed as manufacturing-grade extraction junctions rather than lab-scale interfacial modifiers [123]. Beyond single-junction architectures, SnO_x is gaining importance as a process-enabling buffer in tandem and flexible stacks, where conformity, sputter/process damage tolerance, and mechanical durability are as critical as energy conversion. The flexible perovskite/silicon tandem achieved 33.4% (1 cm^2) and 29.8% on a 260 cm^2 wafer, with minimal losses after bending and thermal cycling. This indicates that SnO_x based buffer/interfacial designs can meet both electrical and mechanical requirements [124]. Lastly, commercial prospects depend on cost-of-ownership, metallization strategy, and

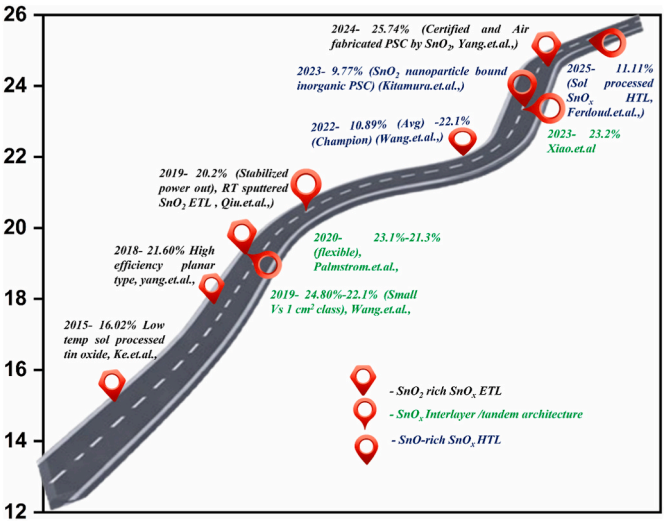

Fig. 7. Performance timeline of SnO_x-based ETL, HTL, and Interlayer architecture devices from 2015 to 2025 [10,35,43,48,84,101,133–135].

lifetime economics, where SnO_x can enable lower-cost electrodes without sacrificing performance. A 2025 J paper shows that a tailored ultrathin SnO_x interlayer can invert the effective polarity at a printed carbon rear electrode in p–i–n PSCs, narrowing the efficiency gap between carbon (21.8%) and Ag (24.0%) while delivering a threefold improvement in projected operational lifetime (>8000 h) and over 60% reduction in materials costs—exactly the kind of quantified trade that can elevate SnO_x from "best-in-class contact layer" to an industrialization enabler for scalable, metal-lean manufacturing lines [125] and Table .5 shows various SnO_x PCE for commercial design.

9. Research gaps and future perspective

Ambipolar SnO_x contacts offer a composition-tunable oxide platform for perovskite solar cells and hold long-term potential for contact applications because of their optical transparency, compositional tunability, and compatibility with diverse device architectures. Still, their mixed-valence and oxygen-nonstoichiometric chemistry creates a central limitation: achieving true ambipolarity without introducing recombination-active tail states, Fermi-level pinning, and time-dependent energetic drift. Many SnO_x films that appear ambipolar in simple electrical tests can behave as recombination-active interlayers in devices because mixed Sn^{2+}/Sn^{4+} phase fractions, oxygen-vacancy populations, and SnO/SnO_2 boundaries generate a sub-gap density of states (DOS) that erode Voc and FF. A practical research gap is therefore the lack of a transferable composition–function map that links measurable descriptors, such as the Sn^{2+}/Sn^{4+} fraction, O/Sn ratio, vacancy signatures, density, surface termination, and sub-gap absorption/tail-state metrics, to device-relevant outputs, including work function and band bending, CBM/VBM offsets, contact resistivity, interfacial recombination velocity, hysteresis, and operational drift across n–i–p, p–i–n, and tandem stacks. Another critical gap, especially for p-type SnO and SnO_x, is the chemical and phase instability of Sn^{2+}-rich films. Because p-type conductivity is associated with SnO-rich compositions, the susceptibility of Sn^{2+} to oxidation can progressively shift the material toward SnO_2-rich regions, alter the work function and hole selectivity, and induce heterojunctions that increase series resistance and recombination. In addition, p-type SnO/SnO_x typically exhibits a narrow fabrication window; even small variations in oxygen activity, plasma chemistry, energetic flux, or thermal budget can significantly alter phase balance, defect density, and transport polarity. These factors create challenges for reproducible large-area processing and practical manufacturability. From a device perspective, p-type SnO and SnO_x also face challenges in achieving sufficiently high hole conductivity, robust band alignment with perovskite absorbers, low interfacial trap density, and operational durability comparable to those of established hole-selective contacts. Thus, SnO_x has realistic long-term potential for practical application because of its inorganic nature, transparency, and compositional tunability, but its viability can depend on overcoming current limitations in phase stability, defect control, charge selectivity, and scalable processing. Although SnO_x-based contacts are promising, they are not yet sufficiently developed for broad practical applications; specifically, phase stability, defect control, and reproducibility remain major unresolved challenges for p-type SnO/SnO_x.

Future work should therefore treat ambipolar SnO_x as a stack-engineered contact system rather than as a single film. Using SnO_x as a bilayer or compositionally graded contact may optimize the bulk region for low-resistance charge transport while engineering the near-surface region as a thin selective skin with lower chemical reactivity and fewer sub-gap defect states. For p-type SnO/SnO_x specifically, research should focus on stabilizing Sn^{2+}-rich hole-selective phases through denser films, diffusion-barrier overlayers, low-temperature capping layers, and targeted passivation strategies that suppress oxidation and defect evolution during operation. Additional progress may be achieved through controlled doping or alloying, interfacial dipole engineering, and hybrid contact designs that improve hole extraction while preserving transparency and low-temperature processability. Equally important is practical device validation beyond peak power conversion efficiency, including film uniformity, contact resistivity, sub-gap and tail states, and long-term durability under maximum power point tracking, damp-heat exposure, and thermal cycling. Under this framework, ambipolar SnO_x, including p-type SnO-like contact layers, could evolve into a practically relevant contact platform for single-junction and tandem perovskite solar cells if the field converges on quantitative metrology and robust process windows that reliably link composition and defect chemistry to selectivity, recombination, and operational stability in realistic device architectures. Fig. 7. A timeline on SnO_x-based ETL, HTL, and interlayer performance.

10. Conclusion

Ambipolar SnO_x is a versatile oxide-contact platform for perovskite solar cells, allowing for modulation of transport polarity, band alignment, and interfacial reactivity by controlling Sn^{2+}/Sn^{4+} speciation and oxygen-related defects. The behavior of film as electron, hole, and ambipolarity is generally decided by the film's actual chemistry and defect structure, more precisely its composition (Sn^{2+}/Sn^{4+} balance, dopants/impurities) and the types and distribution of defects (e.g., oxygen vacancies, tin interstitials, and defect clusters). Unless stoichiometry and valence states are tightly regulated, the same structural or chemical disorder that can enable ambipolarity can also create the density of states, gap states, and trap-assisted recombination, causing time-dependent energetic drift and polarity instability. Reactive sputtering, ALD variations, PLD, and evaporation/CVD-like methods produce various phase fractions, vacancy populations, and surface terminations due to oxygen chemical potentials and energetic fluxes. These changes explain why comparable SnO_x layers have different contact resistivity, recombination losses, and stability. In ETL-mode operation, SnO_2-rich SnO_x exhibits significant electron selectivity, but performance is dependent on oxygen-vacancy management and interfacial trap creation. Although SnO-like or mixed-valence films can enable hole transport in HTL-mode operation, they are susceptible to Sn^{2+} oxidation, interdiffusion, and chemical processes that cause polarity drift. Ambipolar SnO_x is appealing for tandem interlayers, but repeatability involves suppressing mid-gap state creation and maintaining balanced transport. Thus, narrow, measurable process windows linked to valence/defect descriptors, doping/alloying and passivation strategies that decouple conductivity from recombination, and standardised reporting and metrology for composition, energetics, polarity,

and stability under operating stress are necessary to manufacture SnO_x contacts.

Declaration of conflict

No conflict of interest has been reported among authors.

CRediT authorship contribution statement

Neeraja Bose: Formal analysis, Methodology, Resources, Writing – original draft, Writing – review & editing. **Kumar GokulKumar:** Formal analysis, Resources, Software, Validation, Visualization, Writing – review & editing. **Shih Hsuan Chen:** Methodology, Validation, Writing – review & editing. **Kun Mu Lee:** Conceptualization, Funding acquisition, Methodology, Project administration, Supervision, Validation, Writing – review & editing.

Declaration of competing interest

The authors declare that they have no known competing financial interests or personal relationships that could have appeared to influence the work reported in this paper.

Acknowledgement

The authors gratefully acknowledge financial support from the National Science and Technology Council (NSTC), Taiwan, under Project No. NSTC 111-2223-E-182-001-MY4. This research was also supported by Chang Gung University, Taiwan. Project No (URRPD2R0011).

Appendix A. Supplementary data

Supplementary data to this article can be found online at https://doi.org/10.1016/j.mtener.2026.102300.

Data availability

Data will be made available on request.

References

[1] M.A. Green, E.D. Dunlop, M. Yoshita, N. Kopidakis, K. Bothe, G. Siefer, D. Hinken, M. Rauer, J. Hohl-Ebinger, X. Hao, Solar cell efficiency tables (Version 64), Prog. Photovoltaics Res. Appl. 32 (2024) 425–441, https://doi.org/10.1002/pip.3831.
[2] Best Research-Cell Efficiency Chart, (n.d.).
[3] J.P. Correa-Baena, A. Abate, M. Saliba, W. Tress, T. Jesper Jacobsson, M. Grätzel, A. Hagfeldt, The rapid evolution of highly efficient perovskite solar cells, Energy Environ. Sci. 10 (2017) 710–727, https://doi.org/10.1039/c6ee03397k.
[4] B. Roose, Q. Wang, A. Abate, The role of charge selective contacts in perovskite solar cell stability, Adv. Energy Mater. 9 (2019), https://doi.org/10.1002/aenm.201803140.
[5] C.C. Boyd, R. Cheacharoen, T. Leijtens, M.D. McGehee, Understanding degradation mechanisms and improving stability of perovskite photovoltaics, Chem. Rev. 119 (2019) 3418–3451, https://doi.org/10.1021/acs.chemrev.8b00336.
[6] Y.J. Chang, N.H. Chen, T.Y. Chen, Y.M. Shuang, Y.S. Yen, Enhancing efficiency and stability in perovskite solar cells through blended hole transporting materials incorporating Benzo[g]quinoxaline-Conjugated small molecules, ACS Appl. Energy Mater. 7 (2024) 1287–1297, https://doi.org/10.1021/acsaem.3c02932.
[7] W. Ke, M.G. Kanatzidis, Prospects for low-toxicity lead-free perovskite solar cells, Nat. Commun. 10 (2019), https://doi.org/10.1038/s41467-019-08918-3.
[8] A. Abate, Perovskite solar cells Go lead free, Joule 1 (2017) 659–664, https://doi.org/10.1016/j.joule.2017.09.007.
[9] S.S. Shin, S.J. Lee, S. Il Seok, Metal oxide charge transport layers for efficient and stable perovskite solar cells, Adv. Funct. Mater. 29 (2019), https://doi.org/10.1002/adfm.201900455.
[10] A.F. Palmstrom, G.E. Eperon, T. Leijtens, R. Prasanna, S.N. Habisreutinger, W. Nemeth, E.A. Gaulding, S.P. Dunfield, M. Reese, S. Nanayakkara, T. Moot, J. Werner, J. Liu, B. To, S.T. Christensen, M.D. McGehee, M.F.A.M. van Hest, J. M. Luther, J.J. Berry, D.T. Moore, Enabling flexible All-Perovskite tandem solar cells, Joule 3 (2019) 2193–2204, https://doi.org/10.1016/j.joule.2019.05.009.
[11] S. Pisoni, F. Fu, T. Feurer, M. Makha, B. Bissig, S. Nishiwaki, A.N. Tiwari, S. Buecheler, Flexible NIR-transparent perovskite solar cells for all-thin-film tandem photovoltaic devices, J. Mater. Chem. A Mater 5 (2017) 13639–13647, https://doi.org/10.1039/c7ta04225f.
[12] W. Tress, Perovskite solar cells on the way to their radiative efficiency limit – insights into a success story of high open-circuit voltage and low recombination, Adv. Energy Mater. 7 (2017), https://doi.org/10.1002/aenm.201602358.
[13] M. Kashif, T. Munir, N. Nasir, M. Sharif, A. Shahzad, T. Ahmad, A. Hussain, M. Noreen, First principles study of electronic, elastic and optical properties of SnO under in-plane biaxial strain, Digt. J. Nanomat Biostruct. 14 (2019).
[14] A. Mubeen, A. Majid, M. Alkhedher, E.S.M. Tag-ElDin, N. Bulut, Structural and electronic properties of SnO downscaled to monolayer, Materials 15 (2022), https://doi.org/10.3390/ma15165578.
[15] L. He, Q. Cao, X. Feng, C. Luan, W. Wang, W. Zhao, J. Ma, Structural, optical and electrical properties of epitaxial rutile SnO2 films grown on MgF2 (110) substrates by MOCVD, Ceram. Int. 44 (2018) 869–873, https://doi.org/10.1016/j.ceramint.2017.10.013.
[16] M. Karmaoui, A.B. Jorge, P.F. McMillan, A.E. Aliev, R.C. Pullar, J.A. Labrincha, D. M. Tobaldi, One-step synthesis, structure, and band gap properties of SnO2 nanoparticles made by a low temperature nonaqueous sol-gel technique, ACS Omega 3 (2018) 13227–13238, https://doi.org/10.1021/acsomega.8b02122.
[17] J. Wu, Z. Ying, X. Li, M. Zhang, X. Guo, L. Liu, Y. Sun, H. Ma, Y. Yu, Z. He, Y. Zeng, X. Yang, J. Ye, Surface sulfuration of atomic layer deposited snox for enhanced performance of n–i–p perovskite solar cells, Solar RRL 9 (2025), https://doi.org/10.1002/solr.202400879.
[18] L. Zhang, S. Ming, Y. Xia, W. Lu, Properties and electrical evolution of ambipolar SnOx thin films grown by atomic layer deposition in low temperature range, Vacuum 229 (2024), https://doi.org/10.1016/j.vacuum.2024.113596.
[19] Y. Li, D.J. Singh, M.H. Du, Q. Xu, L. Zhang, W. Zheng, Y. Ma, Design of ternary alkaline-earth metal Sn(II) oxides with potential good p-type conductivity, J. Mater. Chem. C Mater 4 (2016) 4592–4599, https://doi.org/10.1039/c6tc00996d.
[20] K. Li, J. Wang, V.A. Blatov, Y. Gong, N. Umezawa, T. Tada, H. Hosono, A. R. Oganov, Crystal and electronic structure engineering of tin monoxide by external pressure, J. Adv. Ceram. 10 (2021) 565–577, https://doi.org/10.1007/s40145-021-0458-1.
[21] M. GrauŽinyte, S. Goedecker, J.A. Flores-Livas, Towards bipolar tin monoxide: revealing unexplored dopants, Phys. Rev. Mater. 2 (2018), https://doi.org/10.1103/PhysRevMaterials.2.104604.
[22] K.G. Godinho, A. Walsh, G.W. Watson, Energetic and electronic structure analysis of intrinsic defects in SnO2, J. Phys. Chem. C 113 (2009) 439–448, https://doi.org/10.1021/jp807753t.
[23] J.X. Zhong, W.Q. Wu, Y. Zhou, Q. Dong, P. Wang, H. Ma, Z. Wang, C.Y. Yao, X. Chen, G. ling Liu, Y. Shi, D. Bin Kuang, Room temperature fabrication of SnO2 electrodes enabling barrier-free electron extraction for efficient flexible perovskite photovoltaics, Adv. Funct. Mater. 32 (2022), https://doi.org/10.1002/adfm.202200817.
[24] S. Idrissi, L. Bahmad, A. Benyoussef, Electronic Properties of the Rutile-type Dioxide SnO2 Material Doped by Sulfur Element: DFT Study, n.d.
[25] K. Rahimi, A. Rawal, Y.F. Zhu, J.N. Hart, E.C. Lovell, J. Scott, Defect engineering in SnO2 catalysts for the organic oxidation reaction, Appl. Catal. B 359 (2024), https://doi.org/10.1016/j.apcatb.2024.124515.
[26] Y. Li, Q. Xin, L. Du, Y. Qu, H. Li, X. Kong, Q. Wang, A. Song, Extremely sensitive dependence of SnOx film properties on sputtering power, Sci. Rep. 6 (2016), https://doi.org/10.1038/srep36183.
[27] R. Barros, K.J. Saji, J.C. Waerenborgh, P. Barquinha, L. Pereira, E. Carlos, R. Martins, E. Fortunato, Role of structure and composition on the performances of P-type tin oxide thin-film transistors processed at low-temperatures, Nanomaterials 9 (2019), https://doi.org/10.3390/nano9030320.
[28] J. Shen, X. Ge, Q. Ge, N. Li, Y. Wang, X. Liu, J. Tao, T. He, S. Yang, Improvement of photovoltaic performance of perovskite solar cells by synergistic modulation of SnO2 and perovskite via interfacial modification, ACS Appl. Mater. Interfaces 16 (2024) 24748–24759, https://doi.org/10.1021/acsami.4c03595.
[29] A. Hultqvist, T.J. Jacobsson, S. Svanström, M. Edoff, U.B. Cappel, H. Rensmo, E. M.J. Johansson, G. Boschloo, T. Törndahl, SnOxAtomic layer deposition on bare perovskite - an investigation of initial growth dynamics, interface chemistry, and solar cell performance, ACS Appl. Energy Mater. 4 (2021) 510–522, https://doi.org/10.1021/acsaem.0c02405.
[30] O.M. Berengue, A.J. Chiquito, Direct evidence of traps controlling the carriers transport in SnO2 nanobelts, Journal of Semiconductors 38 (2017), https://doi.org/10.1088/1674-4926/38/12/122001.
[31] G.W. Watson, Origin of the electron distribution in SnO, J. Chem. Phys. 114 (2001) 758–763, https://doi.org/10.1063/1.1331102.
[32] Y. Wu, Z. Tang, G.J. Cruz, Y. Yang, W. Zhang, W. Ren, P. Zhang, Exploiting the stereoelectronic effects for selective tuning of band edge states of α-SnO: GW quasiparticle calculations, Phys. Rev. B 106 (2022), https://doi.org/10.1103/PhysRevB.106.085201.
[33] S. Samson, C.G. Fonstad, Defect structure and electronic donor levels in stannic oxide crystals, J. Appl. Phys. 44 (1973) 4618–4621, https://doi.org/10.1063/1.1662011.
[34] A. Agresti, F. Di Giacomo, S. Pescetelli, A. Di Carlo, Scalable deposition techniques for large-area perovskite photovoltaic technology: a multi-perspective review, Nano Energy 122 (2024), https://doi.org/10.1016/j.nanoen.2024.109317.
[35] L. Qiu, Z. Liu, L.K. Ono, Y. Jiang, D.Y. Son, Z. Hawash, S. He, Y. Qi, Scalable fabrication of stable high efficiency perovskite solar cells and modules utilizing room temperature sputtered SnO2 electron transport layer, Adv. Funct. Mater. 29 (2019), https://doi.org/10.1002/adfm.201806779.

[36] M. Kam, Q. Zhang, D. Zhang, Z. Fan, Room-temperature sputtered SnO 2 as robust electron transport layer for air-stable and efficient perovskite solar cells on rigid and flexible substrates, Sci. Rep. 9 (2019), https://doi.org/10.1038/s41598-019-42962-9.
[37] R.D. Raninga, R.A. Jagt, S. Béchu, T.N. Huq, W. Li, M. Nikolka, Y.H. Lin, M. Sun, Z. Li, W. Li, M. Bouttemy, M. Frégnaux, H.J. Snaith, P. Schulz, J.L. MacManus-Driscoll, R.L.Z. Hoye, Strong performance enhancement in lead-halide perovskite solar cells through rapid, atmospheric deposition of n-type buffer layer oxides, Nano Energy 75 (2020), https://doi.org/10.1016/j.nanoen.2020.104946.
[38] D. Blackburn, T.J. Routledge, M. O'Kane, E.J. Cassella, O.S. Game, T.E. Catley, C. J. Wood, T. McArdle, D.G. Lidzey, Low-temperature, scalable, reactive deposition of tin oxide for perovskite solar cells, Solar RRL 6 (2022), https://doi.org/10.1002/solr.202200263.
[39] M. Chu, S. Jang, H. Yousuf, Z. Pan, J. Zhang, M.N. Aida, R.U. Rahman, D.P. Pham, M.Q. Khokhar, J. Yi, Atomic layer deposition-based ultrathin SnOxBuffer for high passivation quality in silicon heterojunction solar cells, ACS Photonics 12 (2025) 4916–4923, https://doi.org/10.1021/acsphotonics.5c00467.
[40] T. Hu, T. Becker, N. Pourdavoud, J. Zhao, K.O. Brinkmann, R. Heiderhoff, T. Gahlmann, Z. Huang, S. Olthof, K. Meerholz, D. Többens, B. Cheng, Y. Chen, T. Riedl, Indium-free perovskite solar cells enabled by impermeable tin-oxide electron extraction layers, Adv. Mater. 29 (2017), https://doi.org/10.1002/adma.201606656.
[41] C.H. Chiang, H.T. Chen, W.Y. Chen, W.T. Wang, S.P. Feng, C.G. Wu, Tin oxide/amphiphilic polymer double-layered hole transporter for high-efficiency tin perovskite solar modules, Adv. Energy Mater. 14 (2024), https://doi.org/10.1002/aenm.202400346.
[42] L. Pan, P. Liu, S. Ullah, J. Wang, P. Yang, L. Liu, S.-E. Yang, H. Guo, T. Xia, Y. Chen, Investigation of p-type SnO films served as a potential hole-transporting material for highly efficient perovskite solar cells, J. Phys. D Appl. Phys. 53 (2020) 485103, https://doi.org/10.1088/1361-6463/abae33.
[43] W. Ke, G. Fang, Q. Liu, L. Xiong, P. Qin, H. Tao, J. Wang, H. Lei, B. Li, J. Wan, G. Yang, Y. Yan, Lowerature solution-processed tin oxide as an alternative electron transporting layer for efficient perovskite solar cells, J. Am. Chem. Soc. 137 (2015) 6730–6733, https://doi.org/10.1021/jacs.5b01994.
[44] J. Song, E. Zheng, J. Bian, X.F. Wang, W. Tian, Y. Sanehira, T. Miyasaka, Lowerature SnO2-based electron selective contact for efficient and stable perovskite solar cells, J. Mater. Chem. A Mater 3 (2015) 10837–10844, https://doi.org/10.1039/c5ta01207d.
[45] Q. Dong, Y. Shi, K. Wang, Y. Li, S. Wang, H. Zhang, Y. Xing, Y. Du, X. Bai, T. Ma, Insight into perovskite solar cells based on SnO2 compact electron-selective layer, J. Phys. Chem. C 119 (2015) 10212–10217, https://doi.org/10.1021/acs.jpcc.5b00541.
[46] X. Ren, D. Yang, Z. Yang, J. Feng, X. Zhu, J. Niu, Y. Liu, W. Zhao, S.F. Liu, Solution-processed Nb:SnO2 electron transport layer for efficient planar perovskite solar cells, ACS Appl. Mater. Interfaces 9 (2017) 2421–2429, https://doi.org/10.1021/acsami.6b13362.
[47] E.H. Anaraki, A. Kermanpur, L. Steier, K. Domanski, T. Matsui, W. Tress, M. Saliba, A. Abate, M. Grätzel, A. Hagfeldt, J.P. Correa-Baena, Highly efficient and stable planar perovskite solar cells by solution-processed tin oxide, Energy Environ. Sci. 9 (2016) 3128–3134, https://doi.org/10.1039/c6ee02390h.
[48] T. Kitamura, L. Wang, Z. Zhang, A.K. Baranwal, G. Kapil, S.R. Sahamir, Y. Sanehira, H. Bi, T. Ma, Q. Shen, S. Hayase, Sn perovskite solar cells with tin oxide nanoparticle layer as hole transport layer, ACS Energy Lett. 8 (2023) 3565–3568, https://doi.org/10.1021/acsenergylett.3c01448.
[49] F. Ali, N.D. Pham, H.J. Bradford, N. Khoshsirat, K. Ostrikov, J.M. Bell, H. Wang, T. Tesfamichael, Tuning the amount of oxygen vacancies in sputter-deposited SnOx films for enhancing the performance of perovskite solar cells, ChemSusChem 11 (2018) 3096–3103, https://doi.org/10.1002/cssc.201801541.
[50] P. Pinpithak, H.W. Chen, A. Kulkarni, Y. Sanehira, M. Ikegami, T. Miyasaka, Low-temperature and ambient air processes of amorphous SnOx-based mixed halide perovskite planar solar cell, Chem. Lett. 46 (2017) 382–384, https://doi.org/10.1246/cl.161060.
[51] A. Hultqvist, T.J. Jacobsson, S. Svanström, M. Edoff, U.B. Cappel, H. Rensmo, E. M.J. Johansson, G. Boschloo, T. Törndahl, SnOxAtomic layer deposition on bare perovskite - an investigation of initial growth dynamics, interface chemistry, and solar cell performance, ACS Appl. Energy Mater. 4 (2021) 510–522, https://doi.org/10.1021/acsaem.0c02405.
[52] S.J. Han, S. Kim, J. Ahn, J.K. Jeong, H. Yang, H.J. Kim, Composition-dependent structural and electrical properties of p-type SnO:X thin films prepared by reactive DC magnetron sputtering: effects of oxygen pressure and heat treatment, RSC Adv 6 (2016) 71757–71766, https://doi.org/10.1039/c6ra08726d.
[53] K. Watanabe, T. Kawaguchi, S. Aikawa, P-type conversion of distorted SnOxthin film by mild thermal annealing treatment in pure N2environment, AIP Adv. 12 (2022), https://doi.org/10.1063/5.0103337.
[54] J.S. Jung, S.J. Park, J.H. Ye, J.G. Woo, B.S. Bae, E.J. Yun, Optical, structural, and electrical properties of sputter-deposited SnOx thin films, Thin Solid Films 747 (2022), https://doi.org/10.1016/j.tsf.2022.139139.
[55] L. Qiu, Z. Liu, L.K. Ono, Y. Jiang, D.Y. Son, Z. Hawash, S. He, Y. Qi, Scalable fabrication of stable high efficiency perovskite solar cells and modules utilizing room temperature sputtered SnO2 electron transport layer, Adv. Funct. Mater. 29 (2019), https://doi.org/10.1002/adfm.201806779.
[56] Z. Ni, Z. Yu, J. Huang, Unveiling the ambipolar carrier transport property of SnO2−X for multiple-functional interlayers in perovskite solar cells, Appl. Phys. Lett. 119 (2021), https://doi.org/10.1063/5.0066843.
[57] J. Jia, T. Sugane, S.I. Nakamura, Y. Shigesato, P -type conduction mechanism in continuously varied non-stoichimetric SnOxthin films deposited by reactive sputtering with the impedance control, J. Appl. Phys. 127 (2020), https://doi.org/10.1063/5.0005953.
[58] E. Fortunato, R. Barros, P. Barquinha, V. Figueiredo, S.H.K. Park, C.S. Hwang, R. Martins, Transparent p-type SnOx thin film transistors produced by reactive rf magnetron sputtering followed by low temperature annealing, Appl. Phys. Lett. 97 (2010), https://doi.org/10.1063/1.3469939.
[59] E. Erdenebileg, H. Wang, J. Li, N. Singh, H.A. Dewi, N. Tiwari, N. Mathews, S. Mhaisalkar, A. Bruno, Low-temperature atomic layer deposited electron transport layers for Co-Evaporated perovskite solar cells, Solar RRL 6 (2022), https://doi.org/10.1002/solr.202100842.
[60] Y. Kuang, V. Zardetto, R. Van Gils, S. Karwal, D. Koushik, M.A. Verheijen, L. E. Black, C. Weijtens, S. Veenstra, R. Andriessen, W.M.M. Kessels, M. Creatore, Low-temperature plasma-assisted atomic-layer-deposited SnO2 as an electron transport layer in planar perovskite solar cells, ACS Appl. Mater. Interfaces 10 (2018) 30367–30378, https://doi.org/10.1021/acsami.8b09515.
[61] L. Hoffmann, K.O. Brinkmann, J. Malerczyk, D. Rogalla, T. Becker, D. Theirich, I. Shutsko, P. Görrn, T. Riedl, Spatial atmospheric pressure atomic layer deposition of tin oxide as an impermeable electron extraction layer for perovskite solar cells with enhanced thermal stability, ACS Appl. Mater. Interfaces 10 (2018) 6006–6013, https://doi.org/10.1021/acsami.7b17701.
[62] D. Gao, B. Li, Q. Liu, C. Zhang, Z. Yu, S. Li, J. Gong, L. Qian, F. Vanin, K. Schutt, M.A. Davis, A.F. Palmstrom, S.P. Harvey, N.J. Long, J.M. Luther, X. Cheng Zeng, Z. Zhu, Long-term stability in perovskite solar cells through atomic layer deposition of tin oxide, n.d https://www.science.org.
[63] A. Mohamed, H.B. Lee, V.V. Satale, K.J. Ko, B. Tyagi, D.H. Kim, J.W. Kang, Low-temperature ALD-grown SnOx interlayer for scalable and stable p–i–n perovskite solar cells and modules, Sustain. Energy Fuels 10 (2026) 245–257, https://doi.org/10.1039/d5se01332a.
[64] D.E. Gomersall, K.M. Niang, J.D. Parish, Z. Sun, A.L. Johnson, J.L. MacManus-Driscoll, A.J. Flewitt, Multi-pulse atomic layer deposition of p-type SnO thin films: growth processes and the effect on TFT performance, J. Mater. Chem. C Mater 11 (2023) 5740–5749, https://doi.org/10.1039/d3tc00255a.
[65] K.P.S. Zanoni, D. Pérez-Del-Rey, C. Dreessen, N. Rodkey, M. Sessolo, W. Soltanpoor, M. Morales-Masis, H.J. Bolink, Tin(IV) oxide electron transport layer via industrial-scale pulsed laser deposition for planar perovskite solar cells, ACS Appl. Mater. Interfaces 15 (2023) 32621–32628, https://doi.org/10.1021/acsami.3c04387.
[66] W. Soltanpoor, A.E.A. Bracesco, N. Rodkey, M. Creatore, M. Morales-Masis, Low damage scalable pulsed laser deposition of SnO2 for p–i–n perovskite solar cells, Solar RRL 7 (2023), https://doi.org/10.1002/solr.202300616.
[67] M.I. Hossain, P. Chelvanathan, B. Aissa, A. Khandakar, A. Rahman, S. Mansour, Enhanced perovskite solar cells performance with TiOx and SnOx thin films as electron transport layers, Sci. Rep. 15 (2025), https://doi.org/10.1038/s41598-024-83600-3.
[68] Q. Yang, K. Bittkau, B. Klingebiel, T. Kirchartz, U. Rau, K. Ding, Toward the working mechanisms of tin oxide as buffer layer in perovskite/silicon tandem solar cells, Appl. Phys. Rev. 12 (2025), https://doi.org/10.1063/5.0255418.
[69] K.J. Saji, Y.P. Venkata Subbaiah, K. Tian, A. Tiwari, P-type SnO thin films and SnO/ZnO heterostructures for all-oxide electronic and optoelectronic device applications, Thin Solid Films 605 (2016) 193–201, https://doi.org/10.1016/j.tsf.2015.09.026.
[70] G. Xie, H. Li, X. Wang, J. Fang, D. Lin, D. Wang, S. Li, S. He, L. Qiu, Phase segregation and voltage loss mitigated highly efficient perovskite–organic tandem solar cells with a simple ambipolar SnOx interconnecting layer, Adv. Funct. Mater. 33 (2023), https://doi.org/10.1002/adfm.202308794.
[71] J. Kim, K.S. Kim, C.W. Myung, Efficient electron extraction of SnO2 electron transport layer for lead halide perovskite solar cell, NPJ Comput. Mater. 6 (2020), https://doi.org/10.1038/s41524-020-00370-y.
[72] Y. Chen, Q. Meng, L. Zhang, C. Han, H. Gao, Y. Zhang, H. Yan, SnO2-based electron transporting layer materials for perovskite solar cells: a review of recent progress, J. Energy Chem. 35 (2019) 144–167, https://doi.org/10.1016/j.jechem.2018.11.011.
[73] S.Y. Park, K. Zhu, Advances in SnO2 for efficient and stable n–i–p perovskite solar cells, Adv. Mater. 34 (2022), https://doi.org/10.1002/adma.202110438.
[74] V.P. Hoang Huy, T.M.H. Nguyen, C.W. Bark, Recent advances of doped SnO2 as electron transport layer for high-performance perovskite solar cells, Materials 16 (2023), https://doi.org/10.3390/ma16186170.
[75] J. Tian, J. Zhang, X. Li, B. Cheng, J. Yu, W. Ho, Low-temperature-processed Zr/F Co-Doped SnO2 electron transport layer for high-efficiency planar perovskite solar cells, Solar RRL 4 (2020), https://doi.org/10.1002/solr.202000090.
[76] A.A. Eliwi, M. Malekshahi Byranvand, P. Fassl, M.R. Khan, I.M. Hossain, M. Frericks, S. Ternes, T. Abzieher, J.A. Schwenzer, T. Mayer, J.P. Hofmann, B. S. Richards, U. Lemmer, M. Saliba, U.W. Paetzold, Optimization of SnO2electron transport layer for efficient planar perovskite solar cells with very low hysteresis, Mater. Adv. 3 (2022) 456–466, https://doi.org/10.1039/d1ma00585e.
[77] Z. Zou, F. Li, J. Fang, M. Chen, X. Sun, C. Li, J. Tao, G. Liao, J. Zhang, Low-temperature UVO-sintered ZnO/SnO2 as robust cathode buffer layer for ternary organic solar cells, Nanomaterials 12 (2022), https://doi.org/10.3390/nano12183149.
[78] X. Zhang, Y. Rui, Y. Wang, J. Xu, H. Wang, Q. Zhang, P. Müller-Buschbaum, SnO2 nanorod arrays with tailored area density as efficient electron transport layers for perovskite solar cells, J. Power Sources 402 (2018) 460–467, https://doi.org/10.1016/j.jpowsour.2018.09.072.
[79] T. Bu, J. Li, F. Zheng, W. Chen, X. Wen, Z. Ku, Y. Peng, J. Zhong, Y.B. Cheng, F. Huang, Universal passivation strategy to slot-die printed SnO 2 for hysteresis-

free efficient flexible perovskite solar module, Nat. Commun. 9 (2018), https://doi.org/10.1038/s41467-018-07099-9.
[80] Ç. Kılıç, A. Zunger, Origins of coexistence of conductivity and transparency in SnO2, Phys. Rev. Lett. 88 (2002) 955011–955014, https://doi.org/10.1103/PhysRevLett.88.095501.
[81] J. Shen, X. Ge, Q. Ge, N. Li, Y. Wang, X. Liu, J. Tao, T. He, S. Yang, Improvement of photovoltaic performance of perovskite solar cells by synergistic modulation of SnO2 and perovskite via interfacial modification, ACS Appl. Mater. Interfaces 16 (2024) 24748–24759, https://doi.org/10.1021/acsami.4c03595.
[82] G.M. Arumugam, S.K. Karunakaran, C. Liu, C. Zhang, F. Guo, S. Wu, Y. Mai, Inorganic hole transport layers in inverted perovskite solar cells: a review, Nano Select 2 (2021) 1081–1116, https://doi.org/10.1002/nano.202000200.
[83] S. Yu, Z. Xiong, H. Zhou, Q. Zhang, Z. Wang, F. Ma, Z. Qu, Y. Zhao, X. Chu, X. Zhang, J. You, Homogenized NiO x nanoparticles for improved hole transport in inverted perovskite solar cells, n.d. https://www.science.org.
[84] L. Wang, M. Chen, S. Yang, N. Uezono, Q. Miao, G. Kapil, A.K. Baranwal, Y. Sanehira, D. Wang, D. Liu, T. Ma, K. Ozawa, T. Sakurai, Z. Zhang, Q. Shen, S. Hayase, SnOxas bottom hole extraction layer and top in situ protection layer yields over 14% efficiency in Sn-Based perovskite solar cells, ACS Energy Lett. 7 (2022) 3703–3708, https://doi.org/10.1021/acsenergylett.2c01659.
[85] T. Lv, W. Qin, R. Hong, J. You, Y. Lv, L. Liao, C. Jiang, Radiation stability of the p-Type SnOx TFT with Al2O3 and HfO2 passivation layers, ACS Appl. Electron. Mater. 6 (2024) 8748–8756, https://doi.org/10.1021/acsaelm.4c01288.
[86] Z. Pan, Y. Jeong, M.M. Chu, Y. Jang, F. Wang, J. Chen, Y.S. Kim, J.K. Song, M. Q. Khokhar, J. Yi, Enhancing the mobility of p-type SnOx thin-film transistors through doping and plasma treatment, Solid State Electron. 229 (2025), https://doi.org/10.1016/j.sse.2025.109181.
[87] N. Kelaidis, S. Bousiadi, M. Zervos, A. Chroneos, N.N. Lathiotakis, Electronic properties of the Sn1−xPbxO alloy and band alignment of the SnO/PbO system: a DFT study, Sci. Rep. 10 (2020), https://doi.org/10.1038/s41598-020-73703-y.
[88] A. Hultqvist, T.J. Jacobsson, S. Svanström, M. Edoff, U.B. Cappel, H. Rensmo, E. M.J. Johansson, G. Boschloo, T. Törndahl, SnOxAtomic layer deposition on bare perovskite - an investigation of initial growth dynamics, interface chemistry, and solar cell performance, ACS Appl. Energy Mater. 4 (2021) 510–522, https://doi.org/10.1021/acsaem.0c02405.
[89] L. Wang, M. Chen, S. Yang, N. Uezono, Q. Miao, G. Kapil, A.K. Baranwal, Y. Sanehira, D. Wang, D. Liu, T. Ma, K. Ozawa, T. Sakurai, Z. Zhang, Q. Shen, S. Hayase, SnOxas bottom hole extraction layer and top in situ protection layer yields over 14% efficiency in Sn-Based perovskite solar cells, ACS Energy Lett. 7 (2022) 3703–3708, https://doi.org/10.1021/acsenergylett.2c01659.
[90] J. Singh, S. Gora, A. Datta, Boosting hole mobility in p-type SnOx (x < 2) film through Ge incorporation via co-sputtering, J. Vac. Sci. Technol. A 43 (2025), https://doi.org/10.1116/6.0004887.
[91] S. Yu, Z. Xiong, H. Zhou, Q. Zhang, Z. Wang, F. Ma, Z. Qu, Y. Zhao, X. Chu, X. Zhang, J. You, Homogenized NiO x nanoparticles for improved hole transport in inverted perovskite solar cells, n.d. https://www.science.org.
[92] J.Z. Mbese, Advancements in inorganic hole-transport materials for perovskite solar cells: a comparative review, Energies (Basel) 18 (2025), https://doi.org/10.3390/en18092374.
[93] Q.A.K. Nisa, J.H. Kim, Emerging trends in interface processing: a comparative review of conventional and inverted perovskite solar cells, Advances in Industrial and Engineering Chemistry 1 (2025), https://doi.org/10.1007/s44405-025-00013-0.
[94] S. Ahmmed, Y. He, M.E. Kayesh, M.A. Karim, K. Matsuishi, A. Islam, Ce-Doped SnO2 electron transport layer for minimizing open circuit voltage loss in lead perovskite solar cells, ACS Appl. Mater. Interfaces 16 (2024) 32282–32290, https://doi.org/10.1021/acsami.4c05180.
[95] S. Zhang, H. Gu, S.C. Chen, Q. Zheng, KF-Doped SnO2as an electron transport layer for efficient inorganic CsPbI2Br perovskite solar cells with enhanced open-circuit voltages, J. Mater. Chem. C Mater 9 (2021) 4240–4247, https://doi.org/10.1039/d1tc00277e.
[96] H. Ye, Z. Liu, X. Liu, B. Sun, X. Tan, Y. Tu, T. Shi, Z. Tang, G. Liao, 17.78% efficient low-temperature carbon-based planar perovskite solar cells using Zn-doped SnO 2 electron transport layer, Appl. Surf. Sci. 478 (2019) 417–425, https://doi.org/10.1016/j.apsusc.2019.01.237.
[97] G.V. Sannino, A. Pecoraro, P. Maddalena, A. Bruno, P.D. Veneri, M. Pavone, A. B. Muñoz-García, The role of Mg dopant concentration in tuning the performance of the SnO2 electron transport layer in perovskite solar cells, Sustain. Energy Fuels 7 (2023) 4855–4863, https://doi.org/10.1039/d3se00362k.
[98] D.O. Scanlon, G.W. Watson, On the possibility of p-type SnO2, J. Mater. Chem. 22 (2012) 25236–25245, https://doi.org/10.1039/c2jm34352e.
[99] H. He, Z. Xie, Q. Li, J. Li, Q. Zhang, Novel p-type conductivity in SnO2 thin films by Mg doping, J. Alloys Compd. 714 (2017) 258–262, https://doi.org/10.1016/j.jallcom.2017.04.222.
[100] W. Fu, M. Li, J. Li, G. Fang, P. Ye, W. Ea, X. Xiao, H. Wei, B. Liu, Y. Lu, Y. He, Achieving p-type conductivity in wide-bandgap SnO2by a two-step process, Appl. Phys. Lett. 118 (2021), https://doi.org/10.1063/5.0045663.
[101] D. Yang, R. Yang, K. Wang, C. Wu, X. Zhu, J. Feng, X. Ren, G. Fang, S. Priya, S. (Frank) Liu, High efficiency planar-type perovskite solar cells with negligible hysteresis using EDTA-complexed SnO2, Nat. Commun. 9 (2018), https://doi.org/10.1038/s41467-018-05760-x.
[102] W.L.J.S.C.S.G.Y.Q.Y.W.Y.B.Y.J.S.J.Y. Yongqiang Zhang, ITO/SnO2 Interface Defect Passivation via Atomic Layer Deposited Al2O3 for High-Efficiency Perovskite Solar Cells, PSSA Wiley (n.d.).
[103] A.A. Sutanto, P. Caprioglio, N. Drigo, Y.J. Hofstetter, I. Garcia-Benito, V.I. E. Queloz, D. Neher, M.K. Nazeeruddin, M. Stolterfoht, Y. Vaynzof, G. Grancini, 2D/3D perovskite engineering eliminates interfacial recombination losses in hybrid perovskite solar cells, Chem 7 (2021) 1903–1916, https://doi.org/10.1016/j.chempr.2021.04.002.
[104] L. Zhong, C. Liu, S. Lai, B. Li, B. Zheng, X. Zhang, Recent advances in self-assembled molecular application in solar cells, Nanomaterials 14 (2024), https://doi.org/10.3390/nano14090779.
[105] Q. Zhao, B. Zhang, W. Hui, Z. Su, H. Wang, Q. Zhang, K. Gao, X. Zhang, B.H. Li, X. Gao, X. Wang, S. De Wolf, K. Wang, S. Pang, Oxygen vacancy mediation in SnO2 electron transport layers enables efficient, stable, and scalable perovskite solar cells, J. Am. Chem. Soc. 146 (2024) 19108–19117, https://doi.org/10.1021/jacs.4c03783.
[106] F. Fei, Y. Liao, Y. Xu, S. Wang, L. Li, X. Dong, X. Zhou, J. Gao, K. Wang, N. Yuan, J. Ding, Stable inverted perovskite solar cells with efficiency over 23.0% via dual-layer SnO2 on perovskite, ACS Appl. Mater. Interfaces 16 (2024) 24760–24770, https://doi.org/10.1021/acsami.4c02559.
[107] S. Penukula, M.N. Khanal, M. Sharma, M. Parashar, R.A. Kerner, M. Chen, M. A. Davis, R.A. Saha, E. Solano, M.B.J. Roeffaers, J.J. Berry, J.M. Luther, J. A. Steele, A. Palmstrom, V.R. Whiteside, B. Rout, I.R. Sellers, N. Rolston, Barrier layer design reduces top electrode ion migration in perovskite solar cells, EES Solar 1 (2025) 345–355, https://doi.org/10.1039/d5el00051c.
[108] S. Shin, Y. kim, S. Park, Y.H. Bae, J.S. Noh, Rational tuning of SnO2 electron transport layer grown by atomic layer deposition for performance improvement of perovskite solar cells, Sol. Energy 277 (2024), https://doi.org/10.1016/j.solener.2024.112754.
[109] S. Jeong, S. Seo, H. Park, H. Shin, Atomic layer deposition of a SnO2 electron-transporting layer for planar perovskite solar cells with a power conversion efficiency of 18.3%, Chem. Commun. 55 (2019) 2433–2436, https://doi.org/10.1039/c8cc09557d.
[110] Q. Dong, Y. Shi, C. Zhang, Y. Wu, L. Wang, Energetically favored formation of SnO2 nanocrystals as electron transfer layer in perovskite solar cells with high efficiency exceeding 19%, Nano Energy 40 (2017) 336–344, https://doi.org/10.1016/j.nanoen.2017.08.041.
[111] B. Roose, J.P.C. Baena, K.C. Gödel, M. Graetzel, A. Hagfeldt, U. Steiner, A. Abate, Mesoporous SnO2 electron selective contact enables UV-stable perovskite solar cells, Nano Energy 30 (2016) 517–522, https://doi.org/10.1016/j.nanoen.2016.10.055.
[112] C. Wang, Y. Mo, X. Gao, Q. Huang, T. Bu, Q. Li, Y.-B. Cheng, F. Huang, SnO 2 ink engineering for printing efficient flexible perovskite solar modules. https://www.science.org, 2025.
[113] X. Zhang, Y. Zhou, M. Chen, D. Wang, L. Chao, Y. Lv, H. Zhang, Y. Xia, M. Li, Z. Hu, Y. Chen, Novel bilayer SnO2 electron transport layers with atomic layer deposition for high-performance α-FAPbI3 perovskite solar cells, Small 19 (2023), https://doi.org/10.1002/smll.202303254.
[114] Z. Su, D. Xu, Q. Ma, K. Gao, C. Zhang, C. Xing, S. Wang, W. Shi, X. Wang, K. Li, J. Hui, X. Yang, Atomic layer deposited ZnO–SnO2 electron transport bilayer for wide-bandgap perovskite solar cells, Solar RRL 7 (2023), https://doi.org/10.1002/solr.202201026.
[115] Z. Liu, K. Deng, J. Hu, L. Li, Coagulated SnO 2 colloids for high-performance planar perovskite solar cells with negligible hysteresis and improved stability, Angew. Chem. 131 (2019) 11621–11628, https://doi.org/10.1002/ange.201904945.
[116] G. Yang, C. Chen, F. Yao, Z. Chen, Q. Zhang, X. Zheng, J. Ma, H. Lei, P. Qin, L. Xiong, W. Ke, G. Li, Y. Yan, G. Fang, Effective carrier-concentration tuning of SnO2 quantum dot electron-selective layers for high-performance planar perovskite solar cells, Adv. Mater. 30 (2018), https://doi.org/10.1002/adma.201706023.
[117] K. Nose, A.Y. Suzuki, N. Oda, M. Kamiko, Y. Mitsuda, Oxidation of SnO to SnO2 thin films in boiling water at atmospheric pressure, Appl. Phys. Lett. 104 (2014), https://doi.org/10.1063/1.4867654.
[118] S.A. Panda, S. Barala, A. Hazra, S. Gangopadhyay, Formation of all tin oxide p–n junctions (SnO–SnO $_2$) during thermal oxidation of thin Sn films, Physica Status Solidi (a) 223 (2026), https://doi.org/10.1002/pssa.202400698.
[119] J. Ferdous, M.E. Kayesh, W. Jevasuwan, N. Fukata, A. Islam, Solution-processed SnOx as a hole-transporting material for stable Sn-Based perovskite solar cell, Solar RRL 9 (2025), https://doi.org/10.1002/solr.202500047.
[120] G. Xie, H. Li, X. Wang, J. Fang, D. Lin, D. Wang, S. Li, S. He, L. Qiu, Phase segregation and voltage loss mitigated highly efficient perovskite–organic tandem solar cells with a simple ambipolar SnOx interconnecting layer, Adv. Funct. Mater. 33 (2023), https://doi.org/10.1002/adfm.202308794.
[121] H. Zhang, Y. Luo, T.A. Dela Peña, R. Ma, H. Yan, M. Li, M. Suryawanshi, J. Wu, A. Uddin, Latest strategies promoting stable and efficient perovskite, organic, and perovskite-organic tandem solar cells, Adv. Mater. Interfaces 12 (2025), https://doi.org/10.1002/admi.202500204.
[122] N. Tsvetkov, C. Kim, K. Kim, Y. Kim, J. Park, S. Lee, C.E. Seo, S. Lee, E.H. Jung, B. J. Kang, D.H. Kim, J. Jeong, H. Min, Inorganic cation-capped SnO2 for high-performance perovskite solar cells, J. Mater. Chem. A Mater 13 (2025) 22962–22970, https://doi.org/10.1039/d5ta03268g.
[123] J.W. Lee, J.S. Adu, R.E. Agbenyeke, J. Laverock, A. Sheppard, E. Park, Y. Kim, S. Hong, N.J. Jeon, D.J. Fermin, H.H. Park, Ultrathin oxygen deficient SnOx films as electron extraction layers for perovskite solar modules, J. Mater. Chem. A Mater 13 (2024) 4100–4106, https://doi.org/10.1039/d4ta06871h.
[124] Z. Fang, L. Ding, Y. Yang, X. Gu, H. Li, H. Chen, Y. Yin, W. Wang, X. Wu, Z. Rao, L. Ning, D. Yang, H. Zhang, Y. Long, W. Li, F. Zhang, S. Xia, L. Jia, C. Liu, B. Li, B. Liu, S. Ju, W. Du, H. Zhang, Y. Qin, X. Ru, Y. Xu, Y. Lu, Y. He, Z. Li, X. Xu, M. Qu, B. He, J. Liu, X. Zhang, Flexible perovskite/silicon tandem solar cell with a

dual-buffer layer, Nature 649 (2026) 65–72, https://doi.org/10.1038/s41586-025-09835-w.
[125] T. Du, H.U. Dag, Z. Peng, J. Englhard, A. Barabash, H. Zhang, J. Zhang, J. Tan, S. Qiu, L. Dong, M. Wagner, J.A. Hauch, F. Guo, O. Kasian, J. Bachmann, C. J. Brabec, Enhancing the viability of p-i-n perovskite solar cells with printable carbon cathode: origin of polarity inversion, Joule 10 (2026), https://doi.org/10.1016/j.joule.2025.102224.
[126] R. Liu, L. Wang, Y. Fan, Z. Li, S. Pang, UV degradation of the interface between perovskites and the electron transport layer, RSC Adv 10 (2020) 11551–11556, https://doi.org/10.1039/c9ra10960a.
[127] S.A. Johnson, K.P. White, J. Tong, S. You, A. Magomedov, B.W. Larson, D. Morales, R. Bramante, E. Dunphy, R. Tirawat, C.L. Perkins, J. Werner, G. Lahti, C. Velez, M.F. Toney, K. Zhu, M.D. McGehee, J.J. Berry, A.F. Palmstrom, Improving the barrier properties of tin oxide in metal halide perovskite solar cells using ozone to enhance nucleation, Joule 7 (2023) 2873–2893, https://doi.org/10.1016/j.joule.2023.10.009.
[128] H. Min, D.Y. Lee, J. Kim, G. Kim, K.S. Lee, J. Kim, M.J. Paik, Y.K. Kim, K.S. Kim, M.G. Kim, T.J. Shin, S. Il Seok, Perovskite solar cells with atomically coherent interlayers on SnO2 electrodes, Nature 598 (2021) 444–450, https://doi.org/10.1038/s41586-021-03964-8.
[129] P. Wang, J. Zhao, J. Liu, L. Wei, Z. Liu, L. Guan, G. Cao, Stabilization of organometal halide perovskite films by SnO2 coating with inactive surface hydroxyl groups on ZnO nanorods, J. Power Sources 339 (2017) 51–60, https://doi.org/10.1016/j.jpowsour.2016.11.046.
[130] T. Du, H.U. Dag, Z. Peng, J. Englhard, A. Barabash, H. Zhang, J. Zhang, J. Tan, S. Qiu, L. Dong, M. Wagner, J.A. Hauch, F. Guo, O. Kasian, J. Bachmann, C. J. Brabec, Enhancing the viability of p-i-n perovskite solar cells with printable carbon cathode: origin of polarity inversion, Joule 10 (2026), https://doi.org/10.1016/j.joule.2025.102224.
[131] L. Wang, M. Chen, S. Yang, N. Uezono, Q. Miao, G. Kapil, A.K. Baranwal, Y. Sanehira, D. Wang, D. Liu, T. Ma, K. Ozawa, T. Sakurai, Z. Zhang, Q. Shen, S. Hayase, SnOxas bottom hole extraction layer and top in situ protection layer yields over 14% efficiency in Sn-Based perovskite solar cells, ACS Energy Lett. 7 (2022) 3703–3708, https://doi.org/10.1021/acsenergylett.2c01659.
[132] J. Ferdous, M.E. Kayesh, W. Jevasuwan, N. Fukata, A. Islam, Solution-processed SnOx as a hole-transporting material for stable Sn-Based perovskite solar cell, Solar RRL 9 (2025), https://doi.org/10.1002/solr.202500047.
[133] Y. Yang, H. Huang, L. Yan, P. Cui, Z. Lan, C. Sun, S. Du, X. Wang, C. Yao, S. Qu, Q. Zhang, M. Wang, X. Zhao, M. Li, Compatible soft-templated deposition and surface molecular bridge construction of SnO2 enable air-fabricated perovskite solar cells with efficiency exceeding 25.7%, Adv. Energy Mater. 14 (2024) https://doi.org/10.1002/aenm.202400416.
[134] R. Lin, K. Xiao, Z. Qin, Q. Han, C. Zhang, M. Wei, M.I. Saidaminov, Y. Gao, J. Xu, M. Xiao, A. Li, J. Zhu, E.H. Sargent, H. Tan, Monolithic all-perovskite tandem solar cells with 24.8% efficiency exploiting comproportionation to suppress sn(ii) oxidation in precursor ink, Nat. Energy 4 (2019) 864–873, https://doi.org/10.1038/s41560-019-0466-3.
[135] Y. Xiao, T. Huang, N. Chen, P. Chen, D. Luo, X. Jiang, X. Jia, J. Hu, D. Wang, P. Kaienburg, S. Mahesh, A. Jungbluth, R. Su, C. Li, Q. Lou, C. Yang, B. Wang, I. Habib, H. Ye, H. Zhou, H. Li, L. Meng, X. Li, H. Yu, M. Riede, Z.H. Lu, R. Zhu, H. J. Snaith, Improved interconnecting layer for perovskite–organic tandem solar cells, ACS Energy Lett. 10 (2025) 5184–5191, https://doi.org/10.1021/acsenergylett.5c01923.